Case Studies in Construction Materials 23 (2025) e05259

Contents lists available at ScienceDirect

Case Studies in Construction Materials

journal homepage: www.elsevier.com/locate/cscm

Advancing 3D-printed fiber-reinforced concrete for sustainable construction: A comparative optimization based study of hybrid machine intelligence models for predicting mechanical strength and CO_2 emissions

Shijie Liu [a,b,*], Tong Liu [a,b], Muwaffaq Alqurashi [c], Ahmed A. Abdou Elabbasy [d], Nasser Alanazi [e], Pshtiwan Shakor [f,**]

[a] Department of Architecture and Civil Engineering, Lyuliang University, Lishi, Shanxi 033000, China
[b] Lvliang Key Laboratory of Structural Reliability Analysis in Engineering, Lishi, Shanxi 033000, China
[c] Department of Civil Engineering, College of Engineering, Taif University, P.O. Box 11099, Taif 21944, Saudi Arabia
[d] Civil and Architectural Engineering Department, College of Engineering and Computer Sciences, Jazan University, P.O. Box 706, Jazan 45142, Saudi Arabia
[e] Civil Engineering Department, College of Engineering, University of Ha'il, Ha'il 55474, Saudi Arabia
[f] Technical college of Engineering, Sulaimani Polytechnic University, Sulaymaniyah 46001, Iraq

ARTICLE INFO

Keywords:
3D-printed fiber-reinforced concrete
Advanced machine learning
Concrete
Fibers
Construction material
Mechanical Properties
Compressive strenagth

ABSTRACT

With the increasing demand for sustainable and resilient marine infrastructure in marine environments, 3D printing technologies offer a promising solution for fabricating customized, durable components under challenging conditions. 3D-printed fiber-reinforced concrete (3DPFRC) presents significant potential for rapid, waste-reducing construction of complex geometries, making it suitable for marine structures such as sea walls, breakwaters, underwater pipelines, and floating platforms. However, optimizing 3DPFRC for mechanical performance and environmental sustainability remains a complex challenge. This study proposes advanced machine learning (ML) models to simultaneously predict compressive strength and CO_2 emissions of 3DPFRC, enabling both mechanical and environmental performance evaluation. A user-friendly graphical user interface (GUI) was also developed to facilitate practical deployment by engineers without programming expertise. Four hybrid ML models were evaluated: CNN-LSTM, RA-PSO, XGBoost-PSO, and SVM-PSO. RA-PSO outperformed others with an R^2 of 0.9819 (training) and 0.9674 (testing) for compressive strength and 0.97 (training) and 0.94 (testing) for CO_2 emissions, alongside the lowest MSE (48.24 MPa^2) and highest F1-score (0.9519). This superior performance is primarily due to RA-PSO's adaptive parameter tuning and randomized search, which maintain population diversity and prevent premature convergence, enabling the model to capture complex nonlinear interactions in 3DPFRC mix parameters. Sensitivity analysis revealed that water content (34 %), silica fume (30 %), and the water-to-binder ratio (23 %) were the most influential parameters on compressive strength. These findings confirm RA-PSO as a highly reliable tool for optimizing 3DPFRC mix designs while minimizing environmental impact, particularly in Sustainable Marine and Civil Infrastructure Applications.

* Corresponding author at: Department of Architecture and Civil Engineering, Lyuliang University, Lishi, Shanxi 033000, China.
** Corresponding author.
E-mail addresses: liushijie20211013@163.com (S. Liu), pshtiwan.shakor@spu.edu.iq (P. Shakor).

https://doi.org/10.1016/j.cscm.2025.e05259
Received 16 May 2025; Received in revised form 15 August 2025; Accepted 1 September 2025
Available online 3 September 2025

1. Introduction

Concrete is widely used in construction because of its high strength-to-weight ratio, low cost, large range of design options, and fire resistance [1]. Concrete production wastes water, land, and energy and harms the environment [2]. Due to technical innovation and engineering automation, the construction sector is undergoing a tremendous transformation. Building information modeling (BIM) and 3D computer-aided designs (CAD) have been used to automate construction operations [3]. These breakthrough methods and 3D printing technology have led to fully automated processes in engineering, art, medicine, and industry [4]. In 1997, Joseph Pegna pioneered 3D concrete printing, creating hollow concrete constructions [5]. This was a major construction milestone. Thus, digital building methods are more popular for dependable and fast structural construction [6]. The demand for low-rise buildings is the key reason. 3D printing reduces costs by 80 %, waste by 60 %, and production efficiency by 70 % compared to conventional concrete constructions [7]. Due to job site productivity and lower construction time, construction costs have dropped. Due to its appropriateness for space buildings, 3D printing is expected to prove viable for building lunar and Martian dwellings [8]. The military uses 3D concrete to build entrance checkpoints, defensive combat sites, and barrack houses [9]. Engineers and architects may utilize 3D concrete printing to build detailed and beautiful concrete creations due to their creative flexibility, precision, and accuracy [8]. Computer-aided design (CAD) software creates a three-dimensional model for 3D printing [9]. The model is then segmented, and "G-Code (programming language to control printer movements)" is produced to regulate the printing head's concrete extrusion [10]. Computers control the print head and orifice concrete extrusion. As shown in Fig. 1, 3D concrete printing uses extrusion from a nozzle, pumping, and accurate deposition in successive layers to create a three-dimensional object [11]. Self-supporting, shape-retaining extruded concrete does not bind with layers or require formwork. Concrete ink printing, or additive manufacturing, involves layer-based concrete extrusion [12]. Despite its many benefits, 3D concrete printing must be addressed before being extensively used, such as altering component compositions to meet printability standards like workability and constructability [13].

For 3D printing, optimizing the extrudable slurry system's rheology keeps the structure intact following material deposition before hardening[15]. Printed concrete has physical and durability restrictions. More problems arise due to insufficient printing equipment and trained personnel [16]. Regulatory impediments include the requirement to certify printed structures, the need to amend building codes for 3D-printed concrete structures, and material and procedure issues [17]. Understanding the environmental impact of 3D concrete printing (3DCP) constructions is essential to addressing these issues [18]. Compressive strength (CS) is being studied to assess 3DPFRC composite mechanical performance. The greatest CS of any 3DPFRC is 159 MPa for 3DP steel fiber reinforced concrete. Variations in fiber quantity up to 1 % in 3DPFRC showed material anisotropy for loading orientations of 90°, 45°, and 0° relative to the printing direction [19]. The compressive strength in the printing direction is always greater because more material is cast lengthwise [20]. Anisotropic characteristics of 3DPFRC with fiber quantity modifications up to 1 % showed a drop in CS from 3 % to 14 % at 0° to 45° and 12–26 % at 90° [21]. Molded PE-reinforced specimens had lower compressive strength than printed mixes. Adding 1 % glass fibers to printed mixes increased strength by 108 % [22]. More fibers can reduce bulk slurry composite strength when orientated to achieve the required porosity. The main factors affecting 3DPFRC CS are intrinsic and extrinsic [23]. Experimental extrinsic parameters include curing age and loading orientation, whereas intrinsic factors include mix proportion, raw ingredients, sort, quantity, and fiber geometry [24]. This field lacks a universal standard, criteria, or procedure. This deficiency complicates the search for the best mix design to improve 3DPFRC characteristics. Experimental investigations of the intricate link between input features and 3DPFRC mechanical performance are costly and time-consuming [25]. Data-driven methods like machine learning (ML) algorithms can predict 3DPFRC mechanical performance with provided parameters [26]. 3D-printed concrete compressive strength is predicted by nonlinear regression. Advanced methods are needed since simple regression models cannot forecast reliably [27]. Hybrid material components prevent typical regression models from simulating concrete mechanical properties due to mixed design inputs. Predictive models require advanced modeling [11]. Conventional approaches to modeling 3D printing technology typically rely on static empirical equations, which often lack flexibility and fail to generalize effectively to complex or variable environmental conditions [28]. These limitations underscore the increasing relevance of ML algorithms, which excel in handling high-dimensional, nonlinear data and

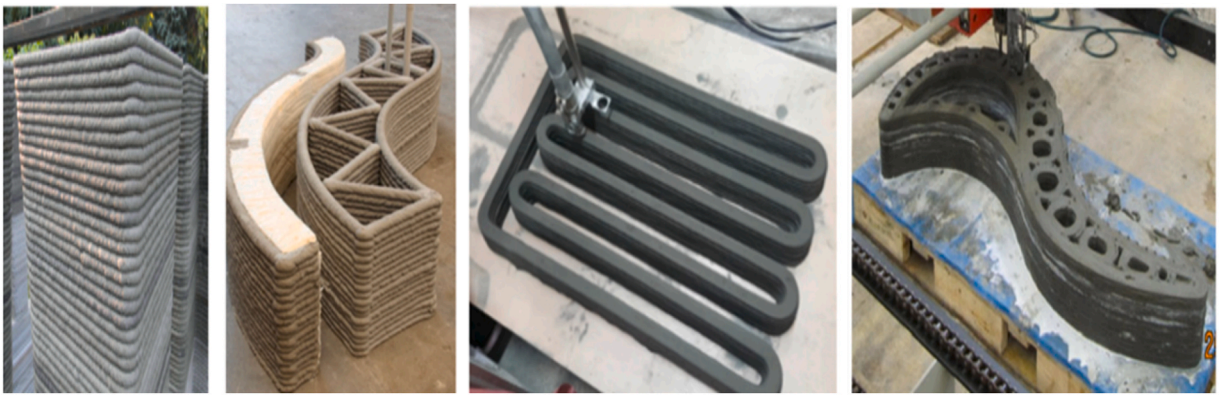

Fig. 1. Three-dimensional extruded concrete models [14].

uncovering intricate relationships among contributing parameters [29]. By learning directly from experimental datasets, ML models offer a robust means of predicting the performance of 3DPFRC under challenging conditions, thereby enhancing the realism and reliability of degradation assessments [30].

With the growing demand for durable and sustainable construction, an intensified interest is in leveraging ML to evaluate the mechanical properties and environmental impacts of extrudable concrete mixes tailored for 3D printing applications [31]. These models efficiently process large datasets and detect subtle patterns affecting compressive strength, setting time, and long-term durability under diverse exposure scenarios [32]. Moreover, ML techniques facilitate a deeper understanding of the interdependencies among material constituents, such as water-to-binder ratio, fiber geometry, and admixture content. These are particularly critical in printable concrete systems designed for layer-by-layer extrusion [33]. Numerous studies have applied ML techniques to assess performance in 3DPFRC applications, such as rapid construction of low-rise buildings, disaster relief shelters, complex architectural forms, and off-Earth construction [7]. These applications demand high accuracy and adaptability, and results show that expanding input variables significantly improves prediction accuracy [34]. Algorithms such as Artificial Neural Networks (ANN) [35], Random Forests (RF), and Support Vector Machines (SVM) have successfully modeled the progressive loss in compressive strength, often outperforming traditional regression approaches due to their data-driven nature and flexibility [2]. Models like XGBoost, linear regression, RF, SVM, Naive Bayes with Backpropagation Neural Networks (NB-BPNN), and Genetic Algorithm-optimized ANN (GA-ANN) have been widely explored, with Deep Neural Networks (DNNs) emerging as powerful tools for high-dimensional, nonlinear concrete modeling tasks [36]. Surrogate DNN models have also been used to optimize superstructure layouts and simulate 3D-printed self-compacting concrete (SCC), yielding significant reductions in material consumption and energy use [37]. To further improve the prediction and optimization of 3D-printable concrete, deep learning frameworks, such as Convolutional Neural Networks (CNN), Recurrent Neural Networks (RNN), and Graph Neural Networks (GNN), have been explored [38]. Although underutilized in construction materials research, hybrid techniques like Adaptive Neuro-Fuzzy Inference Systems (ANFIS) and GA-ANN have proven effective, especially when enhanced through metaheuristic optimizations (e.g., Ant Colony Optimization and Fuzzy C-Means Clustering) to predict the mechanical interface behavior of composite systems such as FRP-concrete[39]. Despite these advancements, challenges remain. Limited datasets hinder model generalization, and cross-validation practices are often inadequate [40]. Moreover, there is a critical research gap in ML-based predictive models that incorporate multi-objective optimization for 3DPFRC while simultaneously accounting for mechanical performance, CO_2 emissions, and production cost [41]. Existing AI applications in this field often focus on strength prediction in isolation, lacking integrated frameworks that reflect the real-world performance demands of 3DPFRC in advanced construction technologies [42,43].

Unlike prior studies that focused solely on single-objective performance prediction, this study uses predictive modeling to provide comprehensive tools for predicting the compressive strength and CO_2 emission of 3D-printable fiber-reinforced concrete to address knowledge gaps. CNN-LSTM, RA-PSO, XGBoost-PSO, and SVM-PSO approaches were used to do this, and their computational concepts were thoroughly explained. CNN-LSTM, RA-PSO, XGBoost-PSO, and SVM-PSO models use an extensive library of experimental datasets collected from multiple peer-reviewed publications to create a universal framework for reliably projecting compressive strength and CO_2 emission of 3DPFRC scenarios. This study employed two categories of statistical metrics. The first type is regression metrics, such as R^2, Adjusted R^2, MSE, AIC, BIC, and log loss, and the second type is classification metrics, such as precision, Recall (Sensitivity), and F1 Score were used to assess and compare the efficacy of all models. Sensitivity analysis assessed input elements on model prediction, such as the Out-of-bag (OOB) feature and Bayesian optimization. Additionally, machine learning can estimate the carbon dioxide emissions for 3DPFRC, leading towards more sustainable construction practices in the rapid prototyping of architectural models. Python was used to construct the GUI based on the model, highlighting the study's originality.

This study offers a dual-contribution framework that addresses both performance prediction and environmental sustainability in 3DPFRC, with direct implications for advanced marine construction. By integrating hybrid machine learning models such as RA-PSO, XGBoost-PSO, CNN-LSTM, and SVM-PSO, this research provides a robust toolset for accurately forecasting compressive strength and CO_2 emissions based on diverse mix design parameters. The findings are significant for marine construction due to the pressing need for durable, form-adaptable, and low-carbon materials in complex aquatic environments. The ability to customize mix designs for strength, durability, and sustainability makes this approach highly suitable for fabricating structural elements exposed to aggressive marine conditions. Furthermore, the development of a user-friendly graphical interface facilitates broader adoption of predictive modeling in engineering practice, allowing design professionals and marine infrastructure developers to optimize concrete formulations without needing advanced coding skills. This enhances the transferability of AI-powered decision-making tools into real-world applications, supporting the creation of resilient, sustainable marine infrastructure.

2. Methodology

2.1. Experimental and analysis dataset

ML models were used to predict the 3DPFRC properties of the datasets from previous publications presented in (Appendix A [43]). Three ML models, such as CNN-LSTM, RA-PSO, XGBoost-PSO, and SVM-PSO, were used to predict compressive strength (CS) and CO_2 emissions. The CS and CO_2 emissions of 3DPFRC were predicted in this work using 16 input factors. Ordinary Portland Cement (OPC) was x1, Sand (S) was x2, Water to Binder ratio (W/B) was x3, Fly Ash (FA) was x4, Ground Slag (GS) was x5, Silica Fume (SF) was x6, Super Plasticizer (SP) was x7, Hydroxypropyl Methylcellulose (HPM) was x8, Water (W) was x9, Fiber Volume Fraction (VF) was x10, Curing Age (CA) was x11, Load Direction (LD) was 12, Fiber Diameter (DF) was x13, Fiber Length (LF) was 14, Aspect Ratio (AR) was x 15 and Fiber Type (FT) was 16. The dataset used in this study includes compressive strength measurements of 3D-printed

fiber-reinforced concrete cube specimens with dimensions of 50 × 50 × 50 mm. Specimens were prepared using a Spectrum Z510 3D printer (Z Corporation) equipped with an HP 4810 A 11 nozzles, capable of producing elements up to 356 mm (length) × 254 mm (width) × 203 mm (height). After printing, specimens were water-cured for 28 days at 20 ± 2 °C and approximately 95 % relative humidity. Compressive strength tests were performed using a 3000 kN capacity hydraulic testing machine at a loading rate of 0.5 MPa/s, in accordance with [**ASTM C109**]. All recorded values correspond to the average of three replicate specimens per mix design, and results were normalized to account for potential size effects when integrating data from other studies. Table 1 shows Pearson's 3DPFRC variables. The models were implemented in collab Google using Python. The statistical analysis properties for 3DPFRC properties are listed in Table 2. Fig. 2 shows how data focuses on various components-compressive strength relationship sections. The OPC (kg/m3) vs CS (MPa) figure shows that compressive strength steadily increases with cement concentration, consistent with the conventional behavior that increased cement content increases compressive strength up to a point.

The W/B vs. CS (MPa) graphic indicates that the water-to-binder ratio decreases compressive strength. This behavior is caused by excess water in the mixture, creating capillary spaces. The SF (kg/m^3) (silica foam) plot shows that compressive strength is maximum at medium silica foam ratios, demonstrating that it has a favorable effect up to a certain concentration, after which potential negative effects like increased viscosity or poor dispersion arise. Multiple high-density regions are found in HPMC, SP, and Vf, causing dispersed and nonlinear effects. This may suggest complex behavior or interactions between components. Including fibers in Lf, Df, and Lf/Df increases compressive strength to variable degrees, depending on length, diameter, and volume ratio. ACI or CEBS equations for concrete strength increase are supported by the CA (days) plot's growing strength trend. F-type and LD (x,y,z) have a weak trend, indicating a weak association or the necessity to analyse them individually or incorporate them into nonlinear models. The data graphs (Fig. 3) show a complex relationship between compressive strength and concrete mix components. Compressive strength is directly affected by cement content, water-to-binder ratio, and curing duration. By concrete science, increasing cement concentration increases compressive strength up to specified limitations, and curing duration increases strength growth over time. Due to greater capillary voids and weaker concrete bonding, raising the water-to-binder ratio dramatically affects compressive strength [44]. When used appropriately, fly ash and silica foam can be beneficial pozzolanic ingredients because their effects rely on their amounts and interactions with other mix components [45].

Chemical additions like SP and HPM did not show a linear connection, highlighting the significance of proper dosage and timing to obtain the desired impact [46]. Fiber length, diameter, and volume percentage showed a dynamic effect on concrete strength. They may boost performance, but exceeding limitations or inadequately distributing them in the combination may diminish strength [47]. The influence of fine and coarse aggregates was complicated and nonlinear, demonstrating that granular characteristics and proportions affect mixture performance[48]. Some graphs also demonstrated that the kind of fiber employed (F-type) reflected the results, suggesting that fiber material qualities may be critical to fiber reinforcement in concrete. Figs. 4 and 5 show the probability and correlation plots with the p-value of 3DPFRC parameters.

2.2. Optimizing hyperparameters with K-fold cross-validation

The complexity of the model and the possibility of overfitting are directly impacted by the careful hyperparameter adjustment needed to improve machine learning model performance [49]. CNN-LSTM, RA-PSO, XGBoost-PSO, and SVM-PSO were hyperparameter tuned using the k-fold cross-validation approach (in this case, k = 5) to lessen overfitting. The database was divided into training and testing segments, comprising 80 % for training and 20 % for testing of the total data [50]. The dataset was divided into five distinct folds, four of which were used for training and the fifth of which was kept aside for validation [51]. Four training folds were used to generate an ML model for each iteration, and the model was compared to the remaining fold[52]. Each fold in this five-step process required one confirmation [53]. These iterations' validation errors (k-fold loss) were averaged to determine the ML model error. Five-fold validation was utilized during training to minimize underfitting and maximize model tweaking. Using Min–Max normalization (Eq. (1) **and (2)**) to normalize parameter values increased the effectiveness of machine learning models. Normalizing data within the range [0,1] enhances model stability and optimizes training efficacy[54].

$$Z = \frac{x - \mu}{\sigma} \tag{1}$$

where Z is the standardized value, x is the original value, μ is the mean, and σ is the standard deviation

$$X = \frac{\text{Feature} - \text{Feature}_{min}}{\text{Feature}_{max} - \text{Feature}_{min}} \tag{2}$$

where $'X'$ is the normalized value, and Feature min and Feature max are the minimum and maximum feature values, respectively.

Adjusted crucial parameters Select the appropriate parameters within a search space to enhance model performance [55]. The ideal configuration and search space are determined by defining hyperparameter values and examining their relationships. The search algorithm selection influences the effectiveness of finding the ideal combination. This study employed Bayesian optimization to identify optimal hyperparameters. CNN-LSTM, RA-PSO, XGBoost-PSO, and SVM-PSO hyperparameter optimization results are in Table 3. To further mitigate the risk of overfitting, additional preventive strategies can be incorporated alongside k-fold cross-validation. For deep learning models such as CNN-LSTM, dropout layers (with rates between 0.2 and 0.5) can be introduced to randomly deactivate neurons during training, thereby improving generalization[56]. Regularization techniques, including L1 and L2 penalties, can be applied to constrain model complexity and prevent overfitting to noise. Moreover, data augmentation, such as

Table 1
Pearson's of 3D-printed fiber-reinforced concrete parameters.

	X1	X2	X3	X4	X5	X6	X7	X8	X9	X10	X11	X12	X13	X14	X15	X16	Y1
X1	–	0.39	0.27	−0.4	−0.4	0.16	0.39	0.01	0.25	−0.25	0.48	−0.24	0.5	0.32	0.4	−0.13	−0.01
X2	0.39	–	−0.23	−0.75	0.53	0.46	0.61	−0.28	−0.4	−0.71	0.48	−0.15	0.22	−0.04	−0.18	0.41	0.35
X3	0.27	−0.23	–	0.3	−0.4	−0.86	−0.39	−0.13	0.82	0.18	−0.13	0.12	0.37	−0.3	0.4	0.03	−0.84
X4	−0.4	−0.75	0.3	–	−0.63	−0.65	−0.37	0.3	0.66	0.79	−0.73	0.14	0.16	−0.13	0.48	0.07	−0.59
X5	−0.4	0.53	−0.4	−0.63	–	0.43	0.11	−0.44	−0.7	−0.62	0.36	0.05	−0.35	−0.3	−0.65	0.19	0.48
X6	0.16	0.46	−0.86	−0.65	0.43	–	0.55	0.05	−0.79	−0.45	0.5	−0.2	−0.25	0.44	−0.35	−0.13	0.94
X7	0.39	0.61	−0.39	−0.37	0.11	0.55	–	0.1	−0.23	−0.31	0.28	−0.18	0.29	0.24	0.03	0.07	0.48
X8	0.01	−0.28	−0.13	0.3	−0.44	0.05	0.1	–	0.01	0.39	−0.39	0.14	−0.41	0.85	−0.08	0.12	0.17
X9	0.25	−0.4	0.82	0.66	−0.7	−0.79	−0.23	0.01	–	0.47	−0.32	0.04	0.61	−0.22	0.76	0.08	−0.82
X10	−0.25	−0.71	0.18	0.79	−0.62	−0.45	−0.31	0.39	0.47	–	−0.58	0.13	0.03	0.09	0.37	−0.13	−0.37
X11	0.48	0.48	−0.13	−0.73	0.36	0.5	0.28	−0.39	−0.32	−0.58	–	−0.19	0.11	0.03	−0.11	−0.22	0.43
X12	−0.24	−0.15	0.12	0.14	0.05	−0.2	−0.18	0.14	0.04	0.13	−0.19	–	−0.21	0.01	−0.14	0.09	−0.12
X13	0.5	0.22	0.37	0.16	−0.35	−0.25	0.29	−0.41	0.61	0.03	0.11	−0.21	–	−0.4	0.86	0.06	−0.43
X14	0.32	−0.04	−0.3	−0.13	−0.3	0.44	0.24	0.85	−0.22	0.09	0.03	0.01	−0.4	–	−0.13	−0.04	0.49
X15	0.4	−0.18	0.4	0.48	−0.65	−0.35	0.03	−0.08	0.76	0.37	−0.11	−0.14	0.86	−0.13	–	−0.03	−0.48
X16	−0.13	0.41	0.03	0.07	0.19	−0.13	0.07	0.12	0.08	−0.13	−0.22	0.09	0.06	−0.04	−0.03	–	−0.14
Y1	−0.01	0.35	−0.84	−0.59	0.48	0.94	0.48	0.17	−0.82	−0.37	0.43	−0.12	−0.43	0.49	−0.48	−0.14	–

Table 2
The statistical analysis for 3D-printed fiber-reinforced concrete.

Feature	Mode	Range	IQR	Std Error	95 % CI	CV (%)	Spearman ρ	Regression Coef	P-value	F-statistic	Tolerance
OPC (kg/m3)	483.00	827.00	172.00	13.20	553.85–605.83	39.38	0.10	0.00	0.87	0.03	0.00
S (kg/m3)	1074.00	1656.00	729.00	23.99	782.98–877.39	49.96	0.32	0.03	0.00	40.49	0.00
W/B	0.17	0.19	0.09	0.00	0.22–0.23	28.84	−0.85	−535.11	0.00	733.16	0.00
FA (kg/m3)	0.00	1141.10	604.00	23.81	241.65–335.34	142.68	−0.57	−0.06	0.00	156.42	0.00
GS (kg/m3)	0.00	450.00	322.00	9.82	132.48–171.13	111.83	0.47	0.12	0.00	87.65	0.00
SF (kg/m3)	268.00	377.80	268.00	7.64	150.37–180.46	79.90	0.92	0.29	0.00	2217.56	0.00
SP (kg/m3)	10.70	20.00	7.70	0.29	6.21–7.36	74.44	0.55	3.91	0.00	87.77	0.00
HPMC (kg/m3)	0.00	3.80	1.70	0.07	0.60–0.88	165.26	−0.05	5.79	0.00	8.93	0.00
W (kg/m3)	182.00	245.90	151.00	4.90	258.16–277.46	31.65	−0.69	−0.40	0.00	627.35	0.00
Vf (%)	0.02	0.02	0.02	0.00	0.01–0.01	74.98	−0.35	−2097.67	0.00	45.71	0.30
CA (days)	28.00	27.00	0.00	0.48	23.70–25.60	33.92	0.45	2.12	0.00	66.95	0.27
LD (x,y,z)	3.00	3.00	2.00	0.05	2.00–2.20	40.25	−0.12	−5.99	0.03	4.52	0.85
Lf/Df	300.00	1200.00	150.00	14.18	259.55–315.37	85.32	−0.49	−0.07	0.00	66.68	0.00
Df (mm)	20.00	185.00	19.00	2.91	37.12–48.57	117.39	0.04	0.41	0.00	96.39	0.00
Lf (mm)	6.00	18.00	2.00	0.22	7.00–7.87	51.21	−0.54	−5.23	0.00	89.67	0.00
Ftype	2.00	5.00	1.00	0.07	2.25–2.51	47.38	−0.11	−4.97	0.02	5.56	0.13
CS (MPa)	0.00	153.40	68.05	2.39	55.97–65.38	68.11	0.10	−0.05	0.87	0.03	0.05

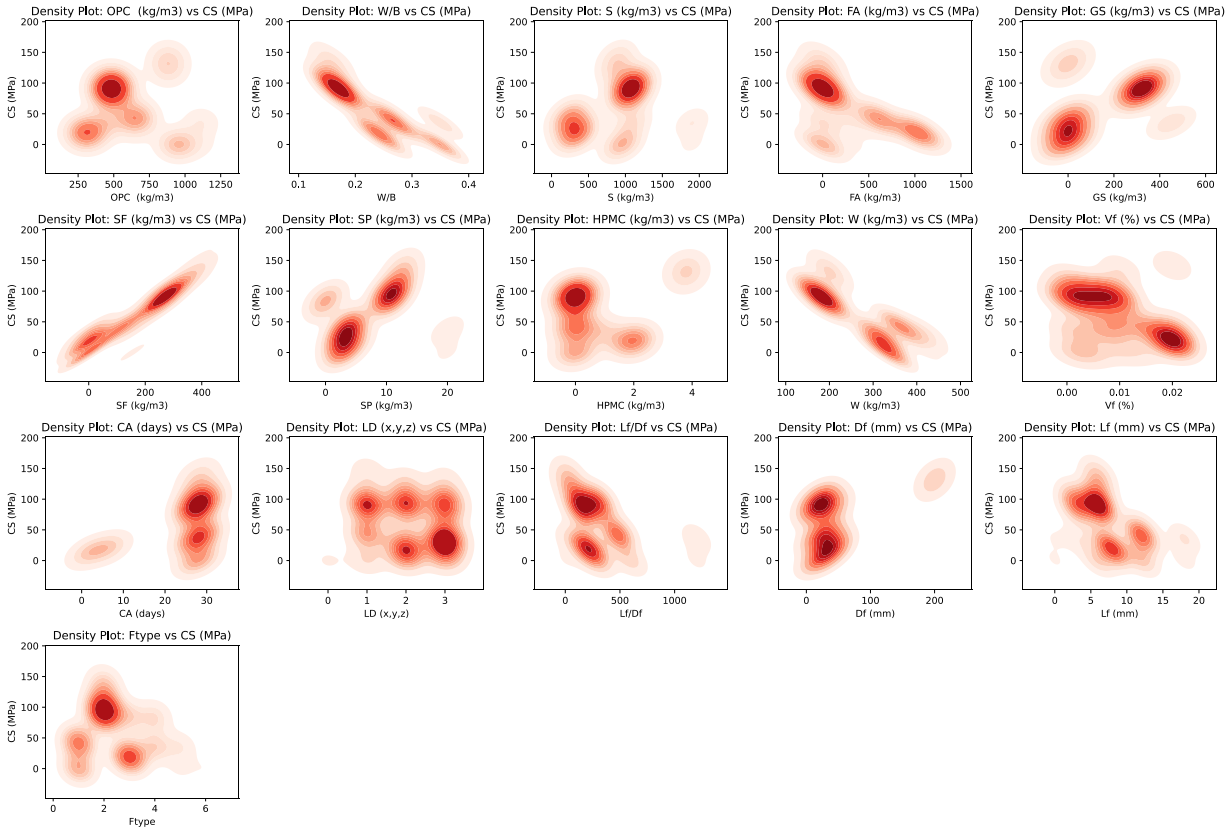

Fig. 2. Bivariate Density Analysis of Compressive Strength versus 3D-printed fiber-reinforced Concrete Mix Components.

generating synthetic samples via bootstrapping or perturbing mix design parameters within realistic engineering limits, can expand the diversity of the training set and enhance model robustness[57]. The choice of PSO over grid or random search was motivated by its ability to efficiently explore large, continuous, and non-convex hyperparameter spaces while avoiding exhaustive computation[58]. Grid search systematically evaluates every possible combination, which becomes computationally expensive and impractical for high-dimensional search spaces[59]. Random search improves efficiency but may still miss promising regions of the search space. In contrast, PSO leverages swarm intelligence to balance exploration and exploitation, enabling faster convergence toward optimal or near-optimal solutions with fewer evaluations[60]. This makes PSO particularly advantageous for tuning SVM hyperparameters, where kernel parameters (e.g., C, γ) interact in complex, nonlinear ways that benefit from adaptive search mechanisms[61].

3. Description of ML models

3.1. Convolutional neural network – long short-term memory (CNN-LSTM)

Utilizing the advantages of both CNN and LSTM, a CNN-LSTM deep learning ensemble model [62]. The first CNN-LSTM layer is a 1000-word embedding with a 10 × 5 output shape [63]. A one-dimensional convolutional layer succeeds this embedding layer. 1DConv employs 128 filters and a 2 × 2 kernel to ascertain the dimensions of the 1D convolution window [64]. The convolutional layer uses the speedier rectified linear unit (ReLU) instead of the sigmoid function. The training and inference time of neural networks is greatly enhanced [65]. Following the convolutional layer, the max-pooling layer downfilters the input representation and removes only pertinent features for processing, using a pool size of two [66]. In the max-pooling layer, CNN output is sent into the LSTM. For little amounts of data, the 100-unit LSTM layer performs better. The LSTM layer condenses the input data into a single prediction following the dense layer [67]. The CNN-LSTM model comprises 200 epochs, utilizes the mean absolute error as the loss function, and employs the Adam optimizer.Table 4 shoow the Architectural configuration of the CNN-LSTM model.

3.2. Support vector machine optimized – particle swarm optimization (SVM-PSO)

The SVM-PSO model is a hybrid approach that enhances regression accuracy by combining Particle Swarm Optimization (PSO) and Support Vector Machines (SVM) [68]. SVM's efficacy in this configuration mostly depends on the ideal hyperparameters, but it creates a nonlinear function to forecast outputs such as compressive strength decline [69]. PSO is employed to autonomously calibrate the

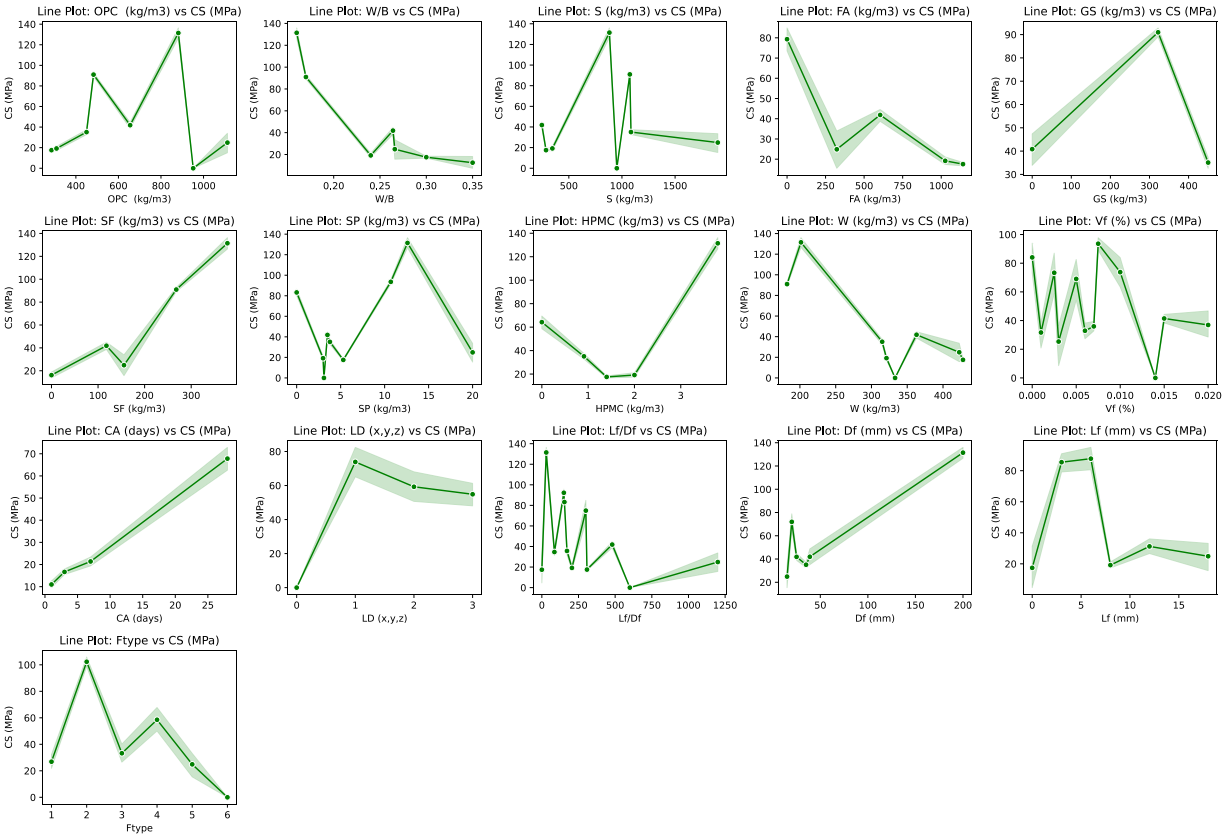

Fig. 3. Line Plots of compressive strength and the other important parameters of 3D-printed fiber-reinforced concrete.

parameters (C, gamma, epsilon) by mimicking the intelligent search behavior of a swarm [70]. This amalgamation improves model generalization and obviates the necessity for human tuning. SVM-PSO is proficient with small to medium datasets and can identify nonlinear patterns using kernel functions [71]. Notwithstanding its advantages, the model necessitates increased processing resources owing to the iterative characteristics of PSO and is susceptible to input scaling. It also exhibits a deficiency in interpretability, which may constrain practical uses [72].

3.3. Randomized adaptive particle swarm optimization (RA-PSO)

The Randomized Adaptive Particle Swarm Optimization (RA-PSO) technique improves convergence and prevents stagnation by combining adaptive control and randomization [73]. This technique adjusts particle placements based on personal and global best experiences and dynamic and stochastic updates to sustain swarm variety [74]. This randomization helps the algorithm avoid local minima. This paper trains an ANN by optimizing weights and biases globally with RA-PSO [73]. A particle represents an ANN configuration, and the fitness function measures the network's prediction error. RA-PSO excels at complex, nonlinear regression applications where gradient-based learning fails [75]. The adaptive process balances Exploration and exploitation, boosting learning stability and convergence reliability. The model's repetitive evaluations over a huge population require a lot of processing power[76]. RA-PSO enhances prediction accuracy but does not provide feature influence interpretability. In this study, RA-PSO modeled compressive strength and CO_2 emissions for 3DPFRC well, making it a valuable tool for uncertain and multivariable engineering problems.

3.4. Extreme gradient boosting optimized – particle swarm optimization (XGBoost-PSO)

The hybrid XGBoost-PSO model combines the high-performance gradient boosting algorithm (XGBoost) with Particle Swarm Optimization's global optimization capabilities [77]. XGBoost captures nonlinear and complicated interactions in structured datasets utilizing decision trees in its ensemble-based technique [78]. Its predictive accuracy depends on choosing appropriate hyper-parameters like learning rate, tree depth, and estimators [79]. This tuning process is automated using PSO to scan the hyperparameter space efficiently. The program learns from individual and collective experience to optimize each particle's arrangement. This integration improves model generalization and reduces manual tuning and grid search [80]. XGBoost-PSO excels in high-dimensional datasets due to its feature importance ranking, multicollinearity resistance, and built-in regularization [81]. When multiple trees

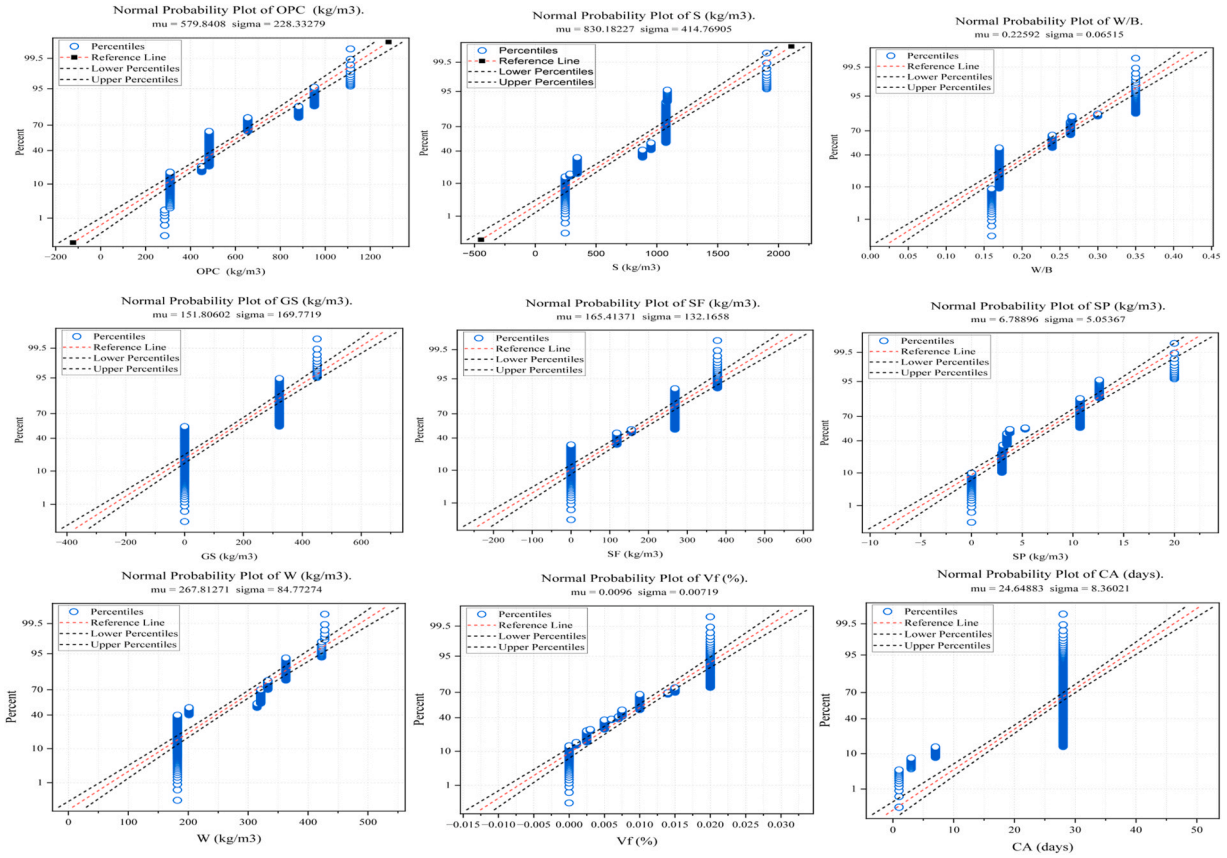

Fig. 4. The probability plots of 3D-printed fiber-reinforced concrete parameters.

are involved, the optimization process might be computationally intensive, and the model may lack clarity [82]. In this study, XGBoost-PSO accurately predicted compressive strength and CO_2 emissions for 3DPFRC, making it a potential tool for application in many structural buildings. Fig. 6 shows the methodology of 3DPFRC prediction using machine learning.

3.5. *Model evaluation indicators*

The statistical metric was divided into two types in this study: the first type is regression metrics, such as R^2, Adjusted R^2, MSE, AIC, BIC, and Log Loss, and the second type is classification metrics, such as Precision, Recall (Sensitivity), and F1 Score. In this work, the classification metrics were applied by discretizing the continuous compressive strength values into two categories ("above median" and "below median"). This supplementary classification evaluation was conducted to assess the models' capability to differentiate between high- and low-performance concrete mixes, which is a critical decision-making factor in practical engineering applications. This dual evaluation framework provides a more comprehensive assessment of both predictive accuracy and practical classification capability. Table 5 lists four indicators for evaluating proposed ML model prediction performance.

4. Results and discussion

4.1. *Receiver operating characteristic and regression error characteristic*

Classification results are compared and visualized with receiver operating characteristic (ROC) and regression error characteristic curves [83]. The Regression Error Characteristic (REC) curve is a generalization of ROC curves to regression. These traits determine the regression model's validity error. For statistical inference, residual differences between expected and actual values must be normal [84]. Unbiased estimations better model performance across strongly correlated predictor variables by detecting and controlling multicollinearity with homoscedasticity constant variation across projected values [85]. Time series regression parameter estimations are less biased with autocorrelation. Outliers and influential points must be identified and addressed to avoid overfitting the model [86]. Valid hypothesis testing and regression analysis predictions require residual normality and linearity evaluation. The REC curves with AUC of all machine learning models are shown in Fig. 7.

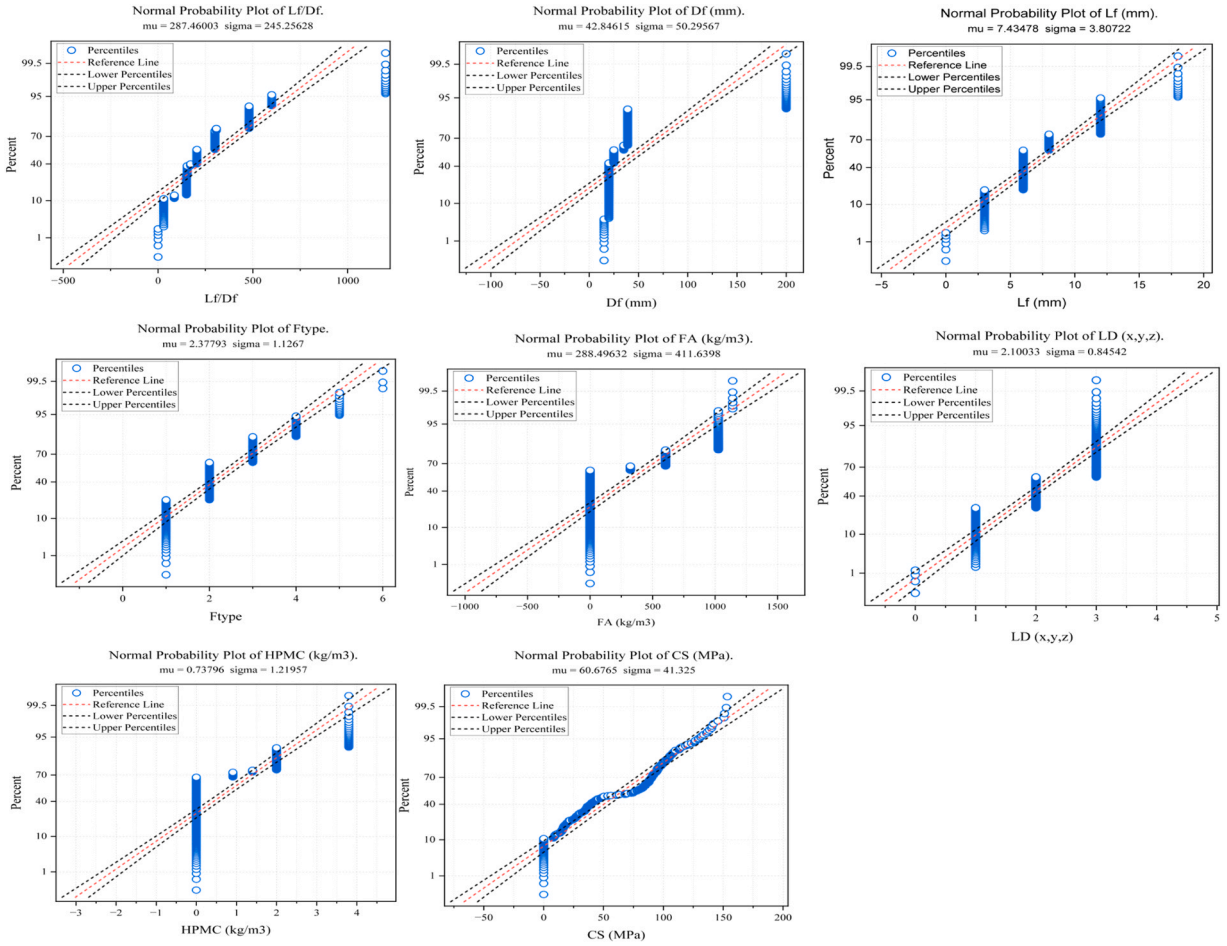

Fig. 4. (*continued*).

As shown in Fig. 7, the area under the curves (AUC) can indicate model quality and accuracy in predicting true values. The SVM-PSO model had the greatest AUC in the training phase, 28.80, indicating its superiority in approximation results during learning. With a few errors, this model covered most of the training data. The SVM-PSO model beat the training model, but the RA-PSO model surpassed all other models in testing with an AUC of 20.99. This indicates that RA-PSO can adapt effectively to shifts in data distribution, maintaining predictive stability where other models show reduced generalization. Most models' AUC values dropped significantly from training to testing, indicating overfitting or data distribution problems. CNN-LSTM declined 43 % and XGBoost-PSO 41.5 % with fresh data, suggesting poor generalization. Testing AUC values for the RA-PSO model were 24 % higher than training. This illustrates its adaptability to fresh data, which may match testing data. Despite a performance drop during testing, the SVM-PSO model maintained consistent results with an AUC of 17.24, 40 % lower than training, demonstrating an acceptable ability to handle unknown data. CNN-LSTM and XGBoost-PSO models declined badly with fresh test data, while SVM-PSO and RA-PSO performed best. The investigation suggests that RA-PSO is optimal for balanced and stable performance and SVM-PSO for training accuracy [87]. The ROC curves and the average curve with AUC of all machine learning models are shown in Fig. 8.

As shown in Fig. 8, The CNN-LSTM, RA-PSO, XGBoost-PSO, and SVM-PSO models performed almost flawlessly during the training phase, with an AUC of 1.00. This indicates a strong correlation with the training data, although it may also suggest possible overfitting. During the testing phase, the models exhibited robust performance with a minor decrease in accuracy. Both CNN-LSTM and SVM-PSO exhibited a reduction in AUC to 0.98, reflecting a decline of approximately 2 %. However, XGBoost-PSO diminished from 1.00 to 0.99, indicating a loss of no more than 1 %, so illustrating its considerable stability. RA-PSO exhibited remarkable flexibility and generalization capability, achieving a complete AUC of 1.00 in training and testing, indicating its proficiency in managing unseen data at the same level as its learning performance [88].

4.2. *k fold cross-validation*

Using K-fold cross-validation helps reduce the amount of model overfitting to a particular dataset segment, which results in a more accurate efficacy evaluation. Models are frequently enhanced by this strategy, which involves dividing them into training and a test to

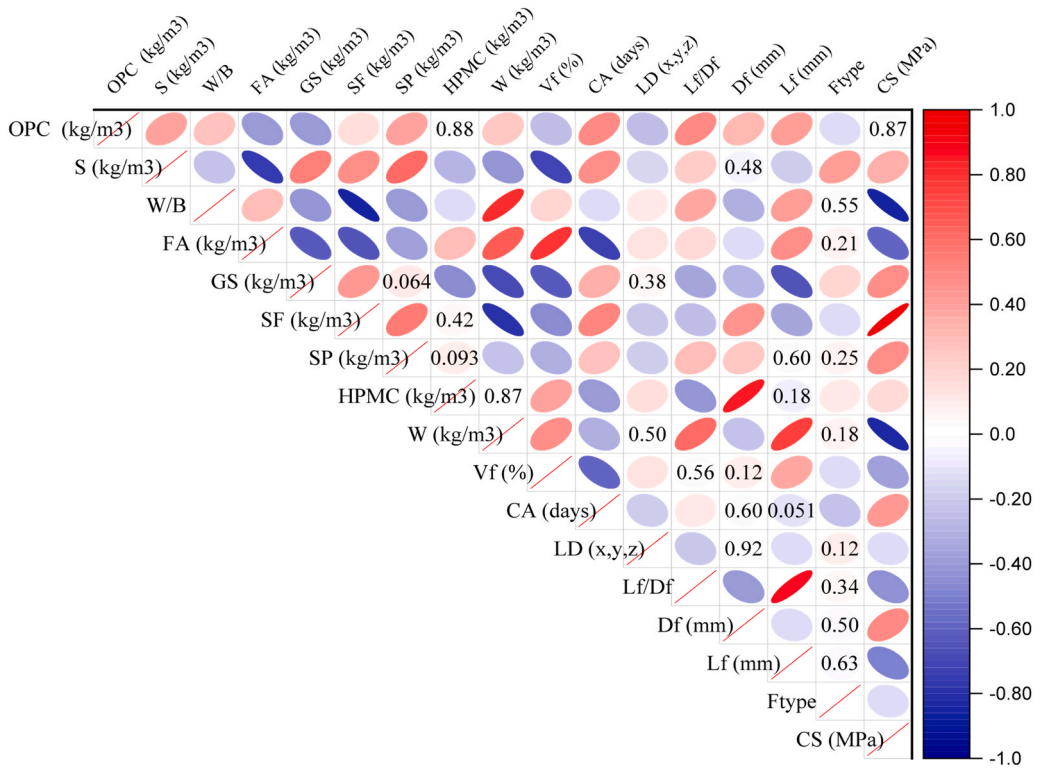

Fig. 5. The correlation plot with p-value (significant level = 0.05) for 3D-printed fiber-reinforced concrete parameters.

Table 3
Tuned key parameters of all models.

Model	Hyperparameter	Value/Range Used in Code	Notes
XGBoost-PSO	learning_rate	[0.01, 0.05, 0.1]	Controls learning speed
	max_depth	[3,5,7]	Tree depth
	n_estimators	[100,200]	Number of boosting rounds
	subsample	[0.8, 1.0]	Sample ratio per round
SVM-PSO	C	[0.1, 1000]	Penalty parameter
	gamma	[1e−4, 1.0]	RBF kernel width
	epsilon	[0.01, 0.3]	Prediction tolerance zone
	kernel	'rbf'	Used fixed
CNN-LSTM	CNN filters	64	Feature extractor
	kernel_size	1	Width of filter
	LSTM units	50	Memory depth
	dropout rate	0.2	Regularization
	dense units	32	Dense layer
	batch size	16	Training batch size
	epochs	100 (early stop)	Max epochs
	optimizer	adam	Adaptive optimizer
RA-PSO	input layer size	auto (based on data)	Input feature count
	hidden neurons	10	Hidden layer size
	output neurons	1	Regression output
	c1	1.5	PSO cognitive param
	c2	1.5	PSO social param
	inertia weight (w)	0.7	PSO inertia factor
	n_particles	30	Swarm size
	iterations	100	PSO iterations

improve performance assessment and avoid overfitting [52]. Through the utilization of this strategy, the dependability and precision of the models were further validated. As shown in Fig. 9, the R^2 values for each of the four models' five folds are displayed [89]. In Fig. 9, the R^2 value for the average of five folds shows that the RA-PSO model performed best for training and testing. RA-PSO achieved the highest accuracy (training: 0.982, testing: 0.967). The model's consistency across all folds reflects its ability to avoid overfitting to specific subsets, ensuring robust performance in repeated sampling scenarios, while XGBoost-PSO and CNN-LSTM showed a

Table 4
Architectural configuration of the CNN-LSTM model used in this study.

Model	Input Shape	No. of Layers	CNN Filter Sizes	Pooling Type	LSTM Units	Activation Functions	Output Dimension
CNN-LSTM	5 × 10	1 Embedding + 1 CNN + 1 Pooling + 1 LSTM + Dense	3 × 3	Max-pooling (2 ×2)	100	Tanh (LSTM states), Sigmoid (gates)	1

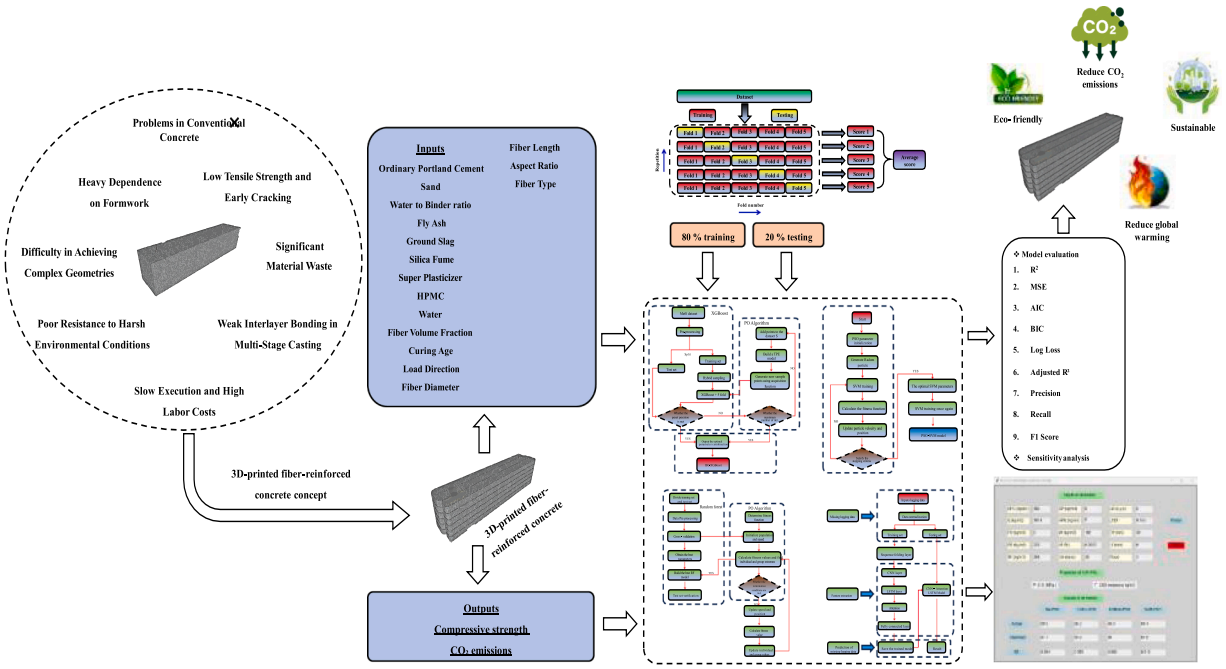

Fig. 6. The Methodology of 3D-printed fiber-reinforced concrete prediction using machine learning.

Table 5
Predictive performance metrics.

Abbreviation	Formula	Descriptions
R^2	$1 - \frac{\sum (y_i - \hat{y}_i)^2}{\sum (y_i - \bar{y})^2}$	y_i: Actual value, $\hat{y}_i$: Predicted value, $\bar{y}$: Mean of actual values, n: Number of samples
MSE	$\frac{1}{n} \Sigma (y_i - \hat{y}_i)^2$	
AIC	$2k - 2\ln(\hat{L})$	k: Number of parameters, $\hat{L}$: Maximum likelihood of the model
BIC	$k \ln(n) - 2\ln(\hat{L})$	
Log Loss	$-(1/n) \Sigma [y_i \log(\hat{p}_i) + (1 - y_i) \log (1 - \hat{p}_i)]$	$\hat{p}_i$: Predicted probability of class 1, y_i: Actual class label (0 or 1), n: Number of samples
Adjusted R^2	$1 - \frac{(1 - R^2)(n - 1)}{(n - p - 1)}$	P: Number of predictors and n: Observations to avoid overfitting
Precision	$\frac{TP}{TP + FP}$	TP: True Positives, FP: False Positives, FN: False Negatives
Recall	$\frac{TP}{TP + FN}$	
F1 Score	$2^* \frac{(Precision \times Recall)}{(Precision + Recall)}$	

well-balanced performance (training: 0.971, testing: 0.945) and (training: 0.955, testing: 0.924), and SVM-PSO had the lowest accuracy (training: 0.949, testing: 0.903) suggesting potential overfitting. Some previous research used k fold = 5 [90,91], and others used k fold = 10 [92].

4.3. Statistical analysis

As shown in Fig. 10, the RA-PSO model consistently beats CNN-LSTM, XGBoost-PSO, and SVM-PSO using statistical criteria including R^2, adiusted_R^2, Precision, Recall, F1_Score, and AOC_AUC. Table 6 shows the optimal and minimum limits for statistical quality coefficients.

The RA-PSO model has the greatest R^2 values of 0.9819 and 0.9674 for the training and testing phases, indicating high predictive accuracy. It accurately detects true positives and minimizes false negatives with a precision (0.9706) and recall (0.934) balance for the testing phase. The model exhibits little performance decline between training and testing, with only a 1.47 % decrease in R^2 score, indicating its generalization potential. The SVM-PSO model has the lowest R^2 values 0.9488 and 0.9031 for training and testing phases among the examined models, indicating lower predictive performance. It shows considerable train-test degradation, with a 4.82 % decline in R^2 score, suggesting overfitting or instability. It also has the lowest recall (0.8519), making it less accurate in identifying

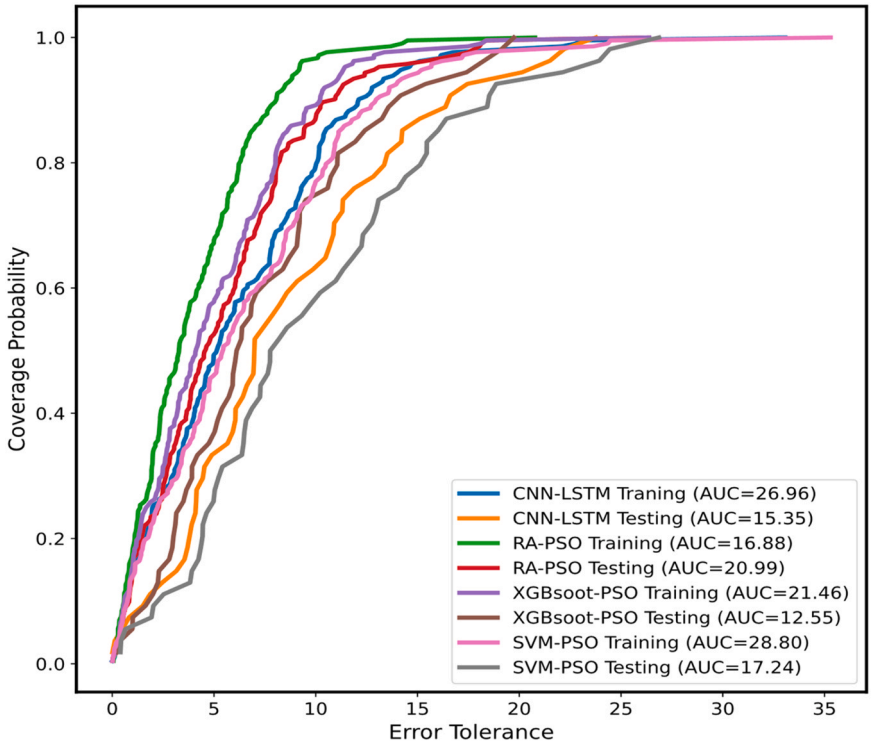

Fig. 7. REC analysis of all models in the training and testing phases.

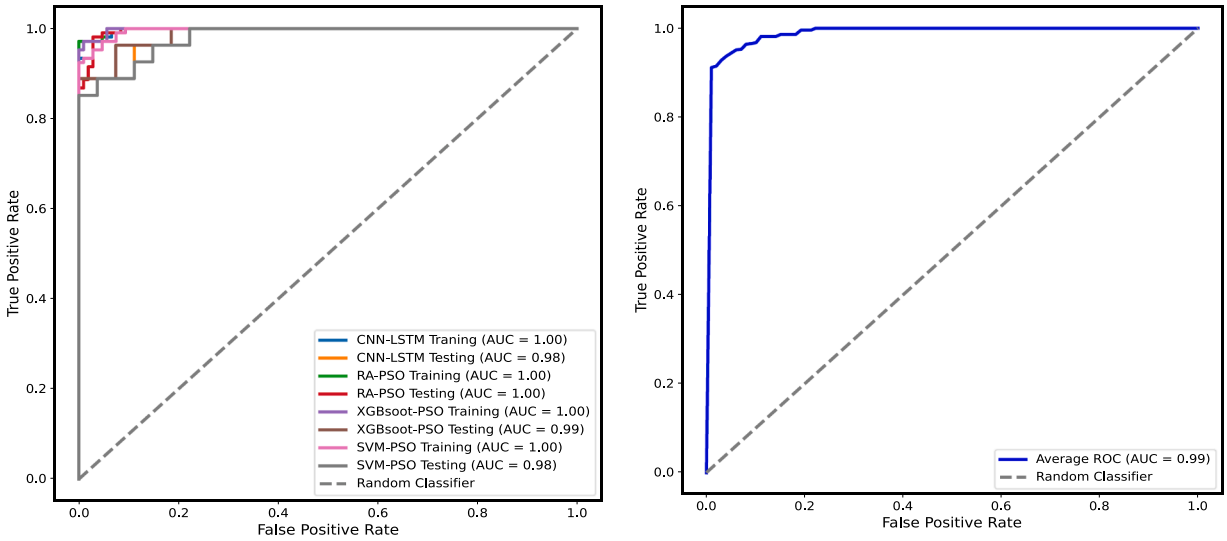

Fig. 8. ROC analysis of all models and average in training and testing phases.

positive cases[95]. The RA-PSO model captures 96.74 % of data variance during testing, proving its predictive potential. However, the XGBoost-PSO model performs 2.68 % worse in testing than in training, raising questions about its generalization capabilities. While XGBoost-PSO achieved perfect precision, its overall performance was slightly lower than RA-PSO in terms of recall and F1-score, indicating that RA-PSO maintained a better balance between precision and generalization. However, the RA-PSO model has the best balance, with 93.4 % recall and a 3.88 % decline between the training and testing phases, demonstrating its consistency. RA-PSO has the highest F1-score (0.9519), beating SVM-PSO by 5.53 %, demonstrating its best precision-recall balance. All models have excellent discrimination, but RA-PSO again leads the group, confirming its reliability. This outcome stems from RA-PSO's global optimization of ANN weights and biases, which enhances regression accuracy while preserving classification performance [96].

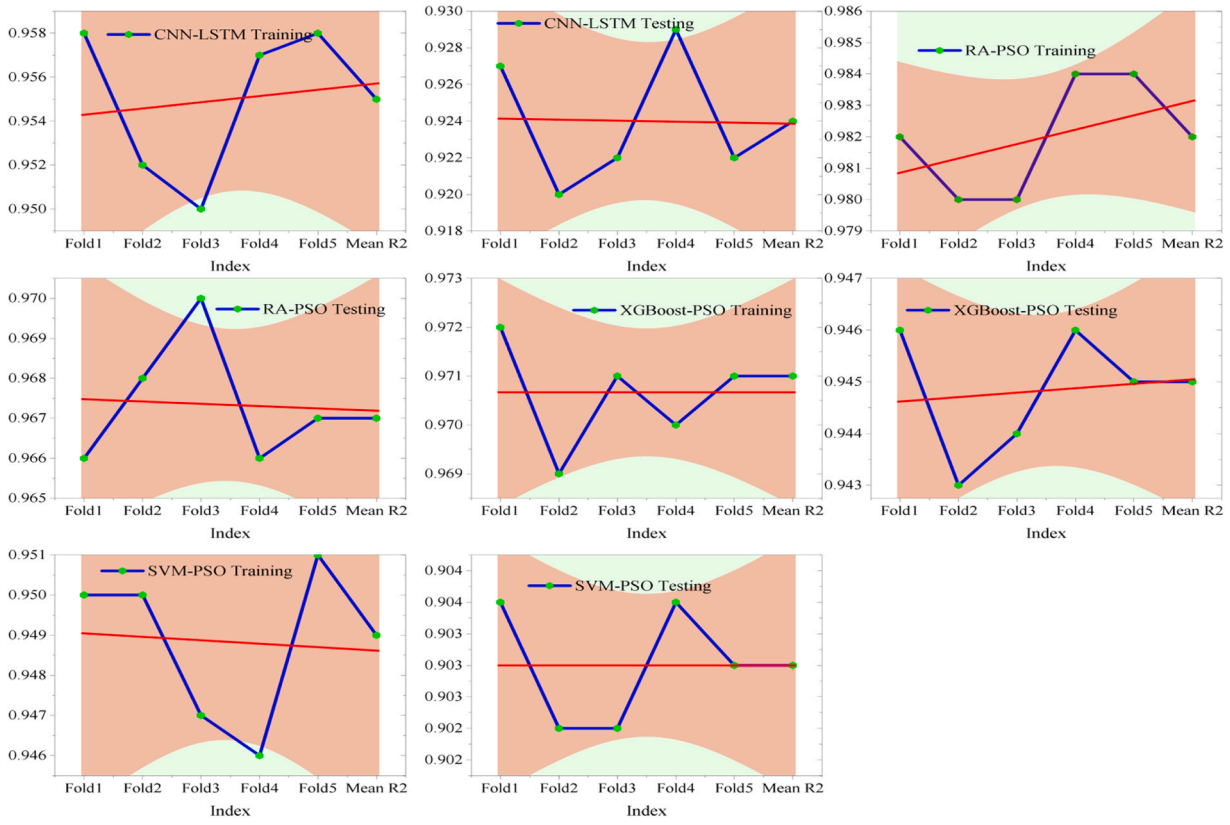

Fig. 9. The R^2 for each fold for all models in the training and testing phases.

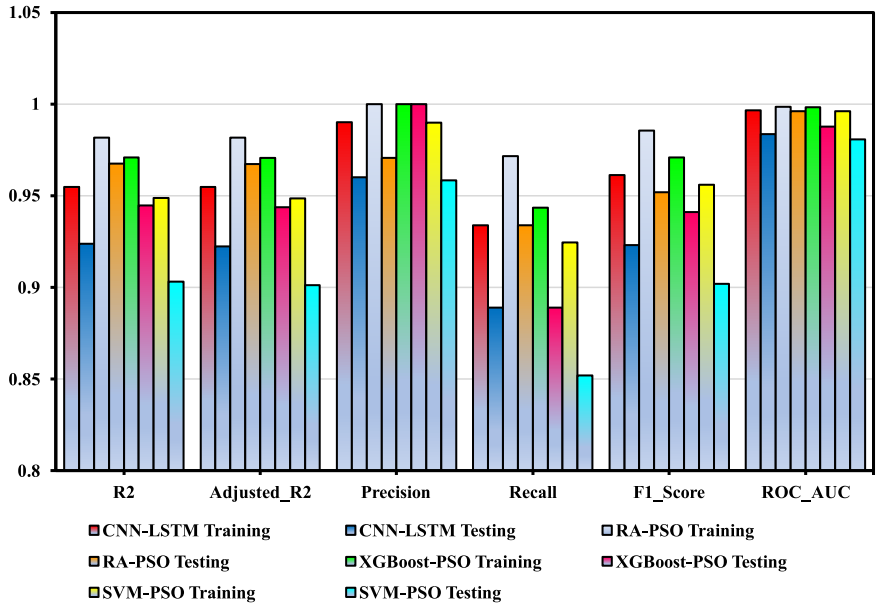

Fig. 10. The R^2, adiusted_R^2, Precision, Recall, F1_Score, and AOC_AUC for all models in the training and testing phases.

XGBoost-PSO loses 5.78 % recall and 3.06 % F1-score between training and testing, the worst overfitting model. High stability and consistent performance with a 1.47 % R^2 drop make RA-PSO trustworthy. RA-PSO (98.3 %) has the highest performance consistency, followed by XGBoost (95.8 %), CNN-LSTM (93.9 %), and SVM (92.6 %), which has better generalization. RA-PSO has a good balance

Table 6
The optimal and minimum limits for statistical quality coefficients.

Metric	Excellent	Very Good	Acceptable	Poor	Unacceptable	Ref.
R^2 (R-Squared)	1	1.0 – 0.9	0.9 – 0.7	0.7 – 0.3	≤ 0.3	[93]
Adjusted R^2	1	1.0 – 0.9	0.9 – 0.6	0.6 – 0.3	≤ 0.3	
Precision	1	1.0 – 0.9	0.9 – 0.8	0.8 – 0.5	≤ 0.5	
Recall	1	1.0 – 0.9	0.9 – 0.7	0.7 – 0.5	≤ 0.5	[94]
F1-Score	1	1.0 – 0.9	0.9 – 0.7	0.7 – 0.5	≤ 0.5	
ROC AUC	1	1.0 – 0.9	0.9 – 0.8	0.8 – 0.5	≤ 0.5	

(97.06 % precision, 93.4 % recall), while XGBoost-PSO has 100 % precision but poorer recall. XGBoost-PSO avoids false positives in precision-critical applications like medical diagnostics despite having 8.89 % lower recall than RA-PSO. RA-PSO's precision (97.06 %), recall (93.4 %), and low train-test variance (1.47 % R^2 decrease) make it ideal for general-purpose applications. The superior generalization capability of the RA-PSO model can be attributed to its adaptive parameter tuning and randomized search strategy, which help maintain diversity in the solution space and avoid premature convergence to local optima. By dynamically balancing exploration and exploitation, RA-PSO effectively captures complex nonlinear relationships between input features and output targets while reducing overfitting. This adaptability enables the model to maintain high predictive accuracy on unseen data, as evidenced by the minimal drop in R^2 (only 1.47 %) from training to testing, compared to larger declines observed in the other models. While CNN-LSTM has a lower R^2 (92.38 %) than PSO-optimized models, it can still generalize complicated data patterns such as sequential or temporal data [97]. As shown in Fig. 11, all models' MSE, AIC, BIC, and Log Loss are in the training and testing phases. The complete investigation demonstrates that the RA-PSO model has the lowest Mean Squared Error (MSE = 48.24) and excellent information criteria (AIC = 829.61, BIC = 836.33) in testing, making it the best choice for accurate predictions. XGBoost-PSO offers remarkable classification accuracy (lowest log loss = 17.78 in training), but its MSE is 62 % higher than RA-PSO, limiting its application. CNN-LSTM performs marginally yet consistently between training and testing. The SVM-PSO model has the highest MSE (137.49) and lowest information criteria (AIC = 269.87), indicating limited generalization. Results demonstrate that RA-PSO is the most accurate, stable, and reliable model. It balances all metrics and has the lowest MSE difference between training and testing (90 %) compared to XGBoost-PSO's 92 %. These advantages make it ideal for most practical accuracy and stability applications [96].

Although the R^2, MSE, and F1-scores obtained by the proposed models are numerically high, statistical inference provides a more rigorous understanding of their reliability. To quantify the uncertainty of these estimates, 95 % confidence intervals (CIs) were computed using bootstrapping with 1000 resamples. For example, the RA-PSO model achieved an R^2 of 0.9674 (95 % CI: 0.9561–0.9772) and an F1-score of 0.9519 (95 % CI: 0.9425–0.9608) in the testing phase, indicating that the observed performance is unlikely to be due to random variation. Paired t-tests comparing RA-PSO against the other models confirmed that its improvement in R^2 and F1-score was statistically significant ($p < 0.05$). This additional statistical evidence reinforces the robustness of the results and supports the practical applicability of the proposed framework.

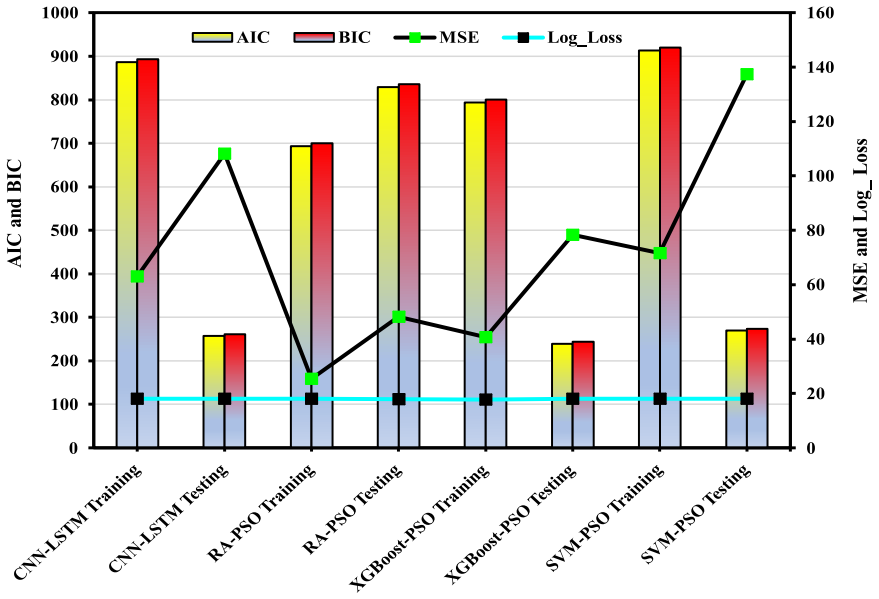

Fig. 11. The MSE, AIC, BIC and Log Loss for all models in the training and testing phases.

4.4. Performance of machine learning

4.4.1. Randomized adaptive particle swarm optimization (RA-PSO)

The construction industry has evolved using 3DPFRC. The compressive strength of these materials directly influences their load-bearing capacity and their ability to maintain performance over time. Compressive strength prediction is problematic due to combining concrete mix properties, fiber type, and printing conditions [43]. The advanced machine learning method, Randomized Adaptive Particle Swarm Optimization (RA-PSO), combines the PSO algorithm with dynamic adaptation and directed randomization additions. Fig. 12 shows the actual and predicted C-S of 3D-printed fiber-reinforced concrete with the RA-PSO model.

The hybrid optimization algorithm-based RA-PSO model accurately predicts 3DPFRC compressive strength. The model's coefficient of determination of 0.9818 for training data and 0.9533 for test data showed its ability to explain compressive strength property fluctuations [98]. While most coefficients were consistent between datasets, the margin of error for the primary parameter (a) increased from ±0.026 in training data to ±0.238 in test data, suggesting potential difficulties in adapting the model to new data. However, a minor decline in the model's accuracy between the training and test datasets while keeping a coefficient of determination over 0.95 confirms its robustness and practicality [99]. As shown in Fig. 13, the confusion matrix results of the RA-PSO model accurately identify 3D-printed concrete compressive strength as below average or above average. Using the training data, the model correctly classified 107 cases as "below average" and 103 as "above average," with only 3 misclassifications in the former and none in the latter. On testing data, accuracy declined to 93.4 % with 7 errors in each category, indicating high generalization but the opportunity for improvement. In training, the model achieved 100 % sensitivity for the "above average" class but dropped to 93.5 % in testing. Both classes demonstrated strong specificity, with 97.3 % in training and 93.4 % for the "below average" class in testing. These results show that the model can categorize compressive strength effectively. Such performance suggests RA-PSO is particularly suited for multivariable engineering problems, where capturing interdependencies between parameters is critical[100]. Table 7 shows the variance analysis (ANOVA) on the performance of a hybrid RA-PSO model in predicting the compressive strength of 3D-printed concrete.

4.4.2. Convolutional neural network - long short-term memory (CNN-LSTM)

The CNN-LSTM model is an advanced hybrid machine learning model that combines CNNs' ability to extract spatial features from data (such as images or signals) with LSTM networks' ability to process time sequences and use long-term context[101]. This integration helps the model analyse complicated geographical and temporal data, such as forecasting structural or material compressive

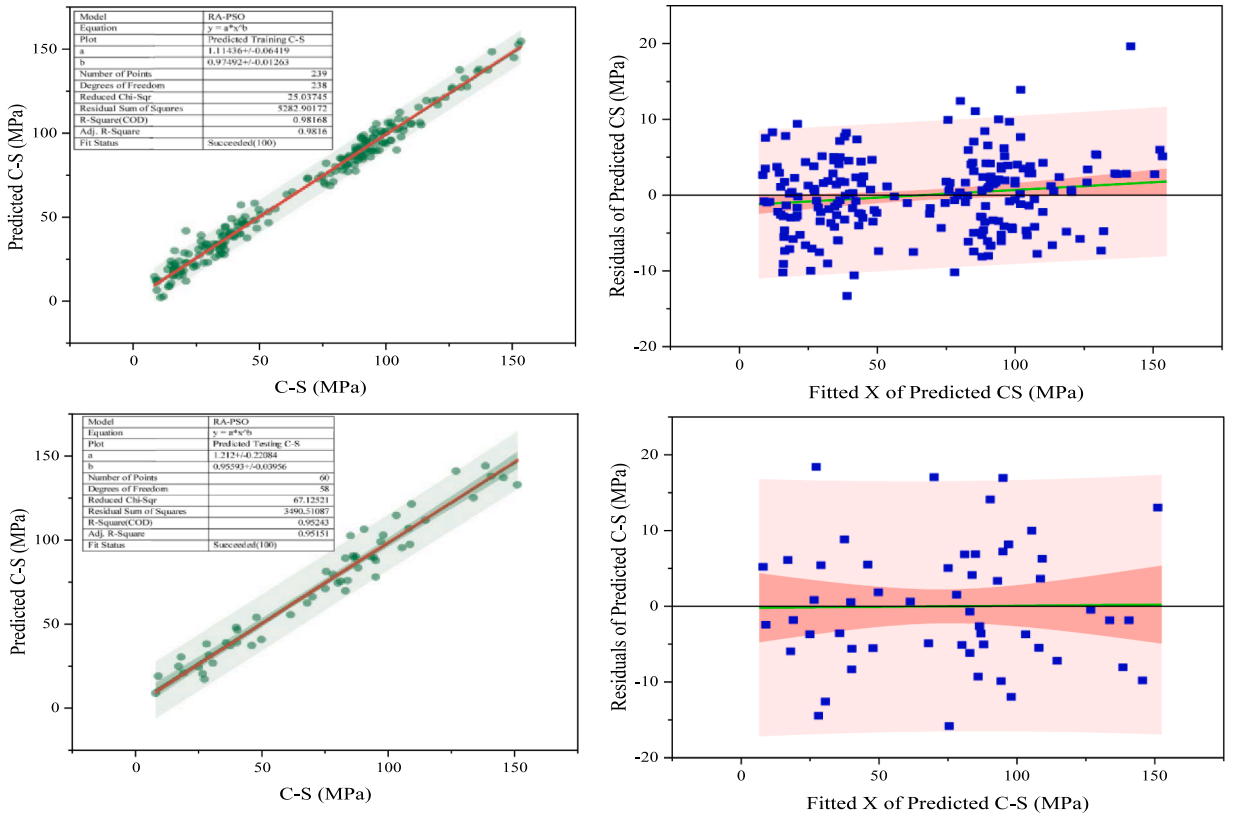

Fig. 12. The actual, predicted, and residual C-S of 3DPFRC with the RA-PSO model.

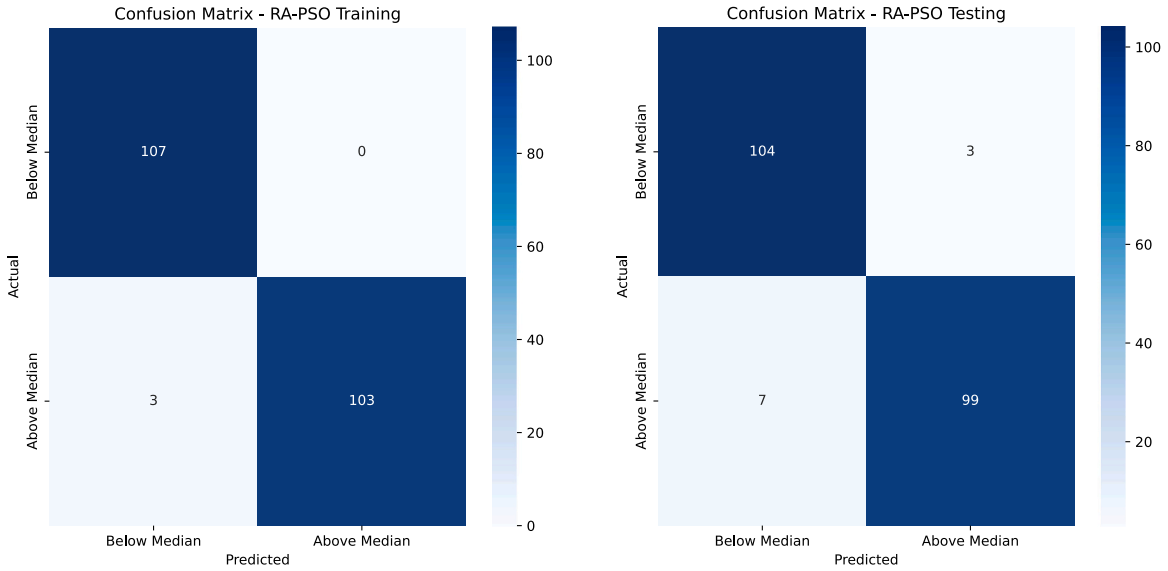

Fig. 13. The confusion matrix results of the RA-PSO model for the training and testing phases.

Table 7
The Analysis of variance (ANOVA) on the performance of a hybrid RA-PSO model in predicting the compressive strength of 3D-printed concrete.

RA-PSO Training						
		DF	SOS	M.S	F Value	Prob>F
Predicted Training C-S (MPa)	Model	1	283204.2	283204.2	11414.9	1.13E−185
Predicted Training C-S (MPa)	Error	211	5234.9	24.8		
Predicted Training C-S (MPa)	Total	212	288439.2			
Fitted Y	Model	1	285813.4	285813.4	4647101.1	0
Fitted Y	Error	211	13.0	0.1		
Fitted Y	Total	212	285826.4			
RA-PSO Testing						
		DF	SOS	M.S	F Value	Prob>F
Predicted Testing C-S (MPa)	Model	1	69918.24	69918.24	1051.87	3.57E−36
Predicted Testing C-S (MPa)	Error	52	3456.47	66.47		
Predicted Testing C-S (MPa)	Total	53	73374.71			
Fitted Y	Model	1	71060.08	71060.08	294354.84	2.92E−99
Fitted Y	Error	52	12.55	0.24		
Fitted Y	Total	53	71072.63			

strength from historical and temporal data[102]. Fig. 14 shows the actual and predicted C-S of 3D-printed fiber-reinforced concrete with the CNN-LSTM model. The CNN-LSTM model accurately predicted the compressive strength of fiber-reinforced concrete, with R^2 values of 0.9553 for training data and 0.9258 for test data, indicating its capacity to explain property changes [103]. While most parameters (e.g., a and b) were consistent between datasets, the margin of error for the main parameter (a) increased from ±0.11333 in training data to ±0.10889 in test data, suggesting potential issues adapting the model to new data. The model's resilience and practicality are shown by the modest accuracy loss between training and test data while retaining a coefficient of determination over 0.92. As shown in Fig. 15, the confusion matrix results of the CNN-LSTM model accurately identify 3D-printed concrete compressive strength as below average or above average[104]. The CNN-LSTM model exhibited great accuracy in categorizing the compressive strength of fiber-reinforced concrete, accurately identifying 106 instances as "below average" and 99 instances as "above average," with merely 7 classification mistakes. Notwithstanding these favorable outcomes, certain flaws signify the necessity to enhance the model's precision when utilized with novel data [105]. This validates its efficacy, although further work is required for superior performance. Table 8 shows the variance analysis (ANOVA) on the performance of a hybrid CNN-LSTM model in predicting the compressive strength of 3D-printed concrete.

4.4.3. Support vector machine - particle swarm optimization (SVM-PSO)

3DPFRC is a promising solution for next-generation construction. The quality of these materials depends on rigorous analysis of their mechanical properties, especially compressive strength, which is a key component in concrete performance. Thus, the SVM-PSO model provides a comprehensive compressive strength prediction solution[106]. This hybrid model uses the SVM algorithm to handle complicated and nonlinear data and the PSO algorithm to optimize parameters and automatically enhance model performance [107].

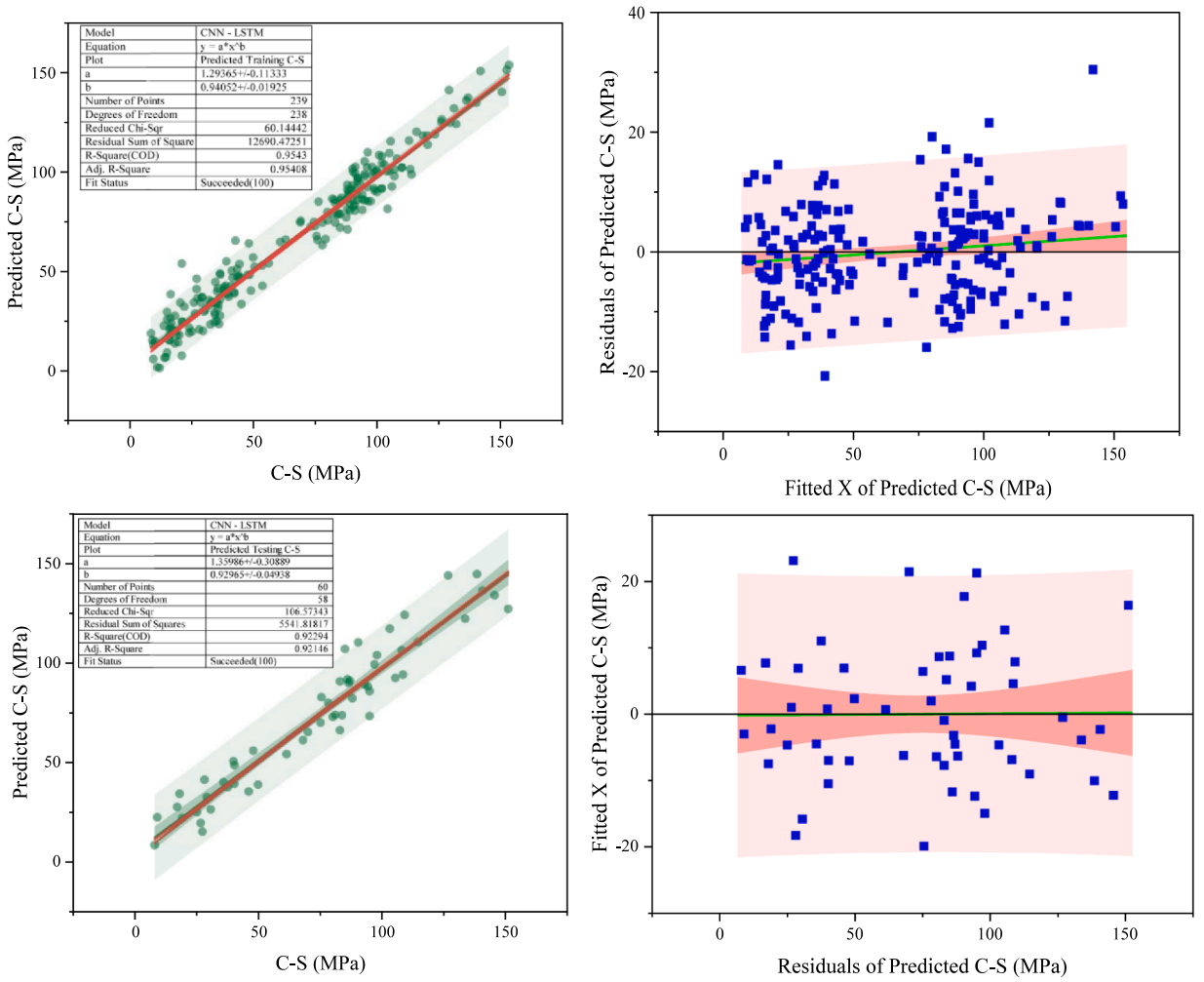

Fig. 14. The actual, predicted, and residuals of C-S of 3D-printed fiber-reinforced concrete with the CNN-LSTM model.

Fig. 16 shows the actual and predicted C-S of 3D-printed fiber-reinforced concrete with SVM-PSO. The SVM-PSO model performed well on training data, with an R^2 value of around 0.9513. This score shows the model's strong learning efficiency by explaining more than 95 % of the training data's variation. In contrast, the model's performance declined on new data, with R^2 dropping to 0.9047. The model overfits the training data and loses accuracy in predicting new data, causing a generalization gap[106]. Graphs indicate the model's projected values closely align with the ideal line (red line), particularly on the training set, indicating accurate data trend simulation[108]. However, residual plot analysis shows significant scatter, especially in test data, where certain values fall beyond the permitted range (red), indicating the model could not represent some occurrences adequately [109]. Technically, the model uses an RBF kernel and over 100 support vectors. This suggests that the model is complicated and makes decisions using much specific data. This improves accuracy but may hinder generalization. Table 9 shows the variance analysis (ANOVA) on the performance of a hybrid SVM-PSO model in predicting the compressive strength of 3D-printed concrete.

Fig. 17 illustrates the SVM-PSO model's two confusion matrices. These matrices assess the model's ability to categorize values into "below median" and "above median" for training and test sets. The model is accurate on the training set (left). This accurately identified 106 cases as "below median" and 98 as "above median." It only misclassified two cases: one "below median" instance as "above median" and eight "above median" instances as "lower." The model learns well and classifies data with 95.9 % accuracy (204 accurate values out of 213 cases). The model accurately classified 26 "below median" and 23 "above median" cases in the test set (right). It only made five errors (one "below" example was "high", and four "above" ones were "low"). Despite this decline, accuracy remained good at 91.7 % (49 out of 54 correct cases). These results show that the SVM-PSO model can distinguish between the two classes in training and testing, boosting its predictive power. In the prior graph analysis, the model's performance on the two sets differed slightly, suggesting overfitting [104].

4.4.4. EXtreme gradient boosting - particle swarm optimization (XGBoost-PSO)

Fig. 18 shows the actual and predicted C-S of 3D-printed fiber-reinforced concrete with XGBoost-PSO. An evaluation of the

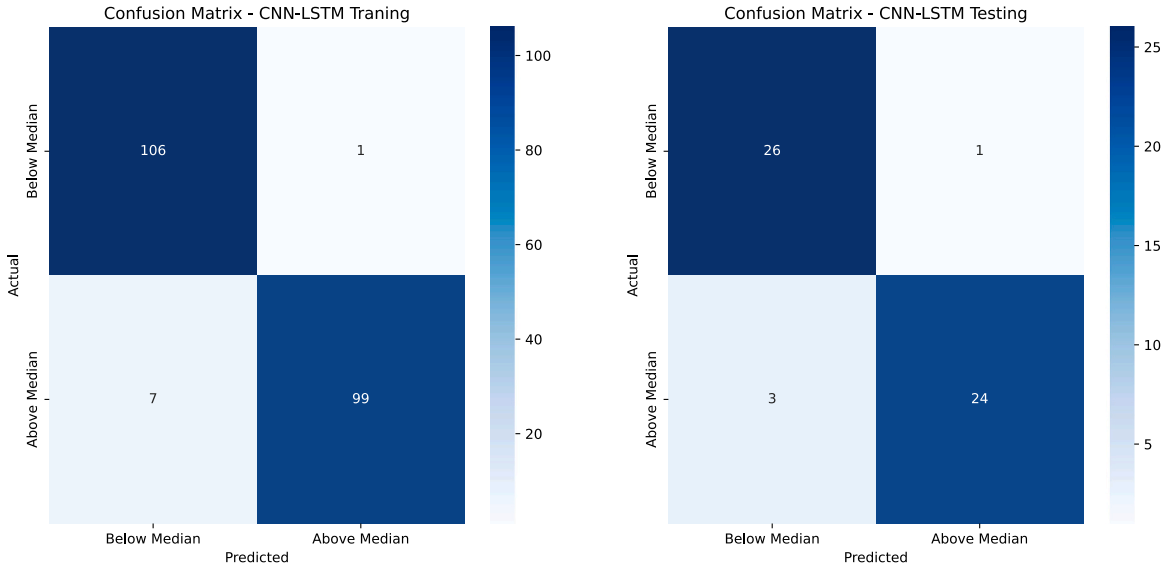

Fig. 15. The confusion matrix results of the CNN-LSTM model for the training and testing phases.

Table 8
The Analysis of variance (ANOVA) on the performance of a hybrid CNN-LSTM model in predicting the compressive strength of 3D-printed concrete.

CNN-LSTM Training						
		DF	SOS	M.S	F Value	Prob>F
Predicted Training C-S	Model	1	265190	265190	4483	4.11E−144
Predicted Training C-S	Error	211	12482	59		
Predicted Training C-S	Total	212	277671			
Fitted Y	Model	1	269972	269972	820222	0
Fitted Y	Error	211	69	0		
Fitted Y	Total	212	270041			
CNN-LSTM Testing						
		DF	SOS	M.S	F Value	Prob>F
Predicted Testing C-S	Model	1	66440.8	66440.82	630.87	9.59E−31
Predicted Testing C-S	Error	52	5476.4	105.32		
Predicted Testing C-S	Total	53	71917.26			
Fitted Y	Model	1	67886.09	67886.01	114685.24	1.28E−88
Fitted Y	Error	52	30.78	0.59		
Fitted Y	Total	53	67916.87			

XGBoost-PSO model's efficacy demonstrates remarkable outcomes regarding accuracy and predictive capability [110]. The model accounted for nearly 97 % of the variation in the training data ($R^2 = 0.9706$) and demonstrated robust performance on the test data, with an R^2 value of around 0.9442, reflecting a minor performance decline of only 2.7 %. The model parameters exhibited notable stability across the training and testing phases, with parameter a falling by merely 1.4 % (from 1.1419 to 1.1259) and parameter b decreasing by 1.37 % (from 0.9612 to 0.948).

Nonetheless, certain challenges were identified in the model's performance, particularly a substantial rise in the reduced chi-square value, which escalated by 97 % on the test data (from 39.63 to 78.16), along with an increase in the margin of error for the parameters, suggesting a necessity for further enhancement[100].

Fig. 19 displays the confusion matrices of the XGBoost-PSO model, assessing its efficacy in categorizing data into two classifications: "Below Median" and "Above Median" for both training and test datasets[111]. The confusion matrix for the training data on the left indicates that the model attained exceptional performance. It accurately categorized 107 samples designated as "Below Median" and committed only 6 errors by misclassifying a sample from the "Above Median" group as "Below Median." Conversely, 100 "Above Median" samples were accurately identified. This signifies an exceptionally high training accuracy of approximately 97.2 %, demonstrating the model's superior capacity to discern patterns from data. In the test data (right side), the model exhibited robust performance, accurately classifying all samples from the "below median" class (27 out of 27 cases), committing only three errors by misclassifying certain samples from the "above median" class as "below," and correctly identifying 24 cases as "above median." This corresponds to an accuracy of roughly 94.4 %, indicating a great performance on the test and showcasing the model's proficiency in generalizations without overfitting. Table 10 shows the variance analysis (ANOVA) on the performance of a hybrid XGBoost-PSO model in predicting the compressive strength of 3D-printed concrete.

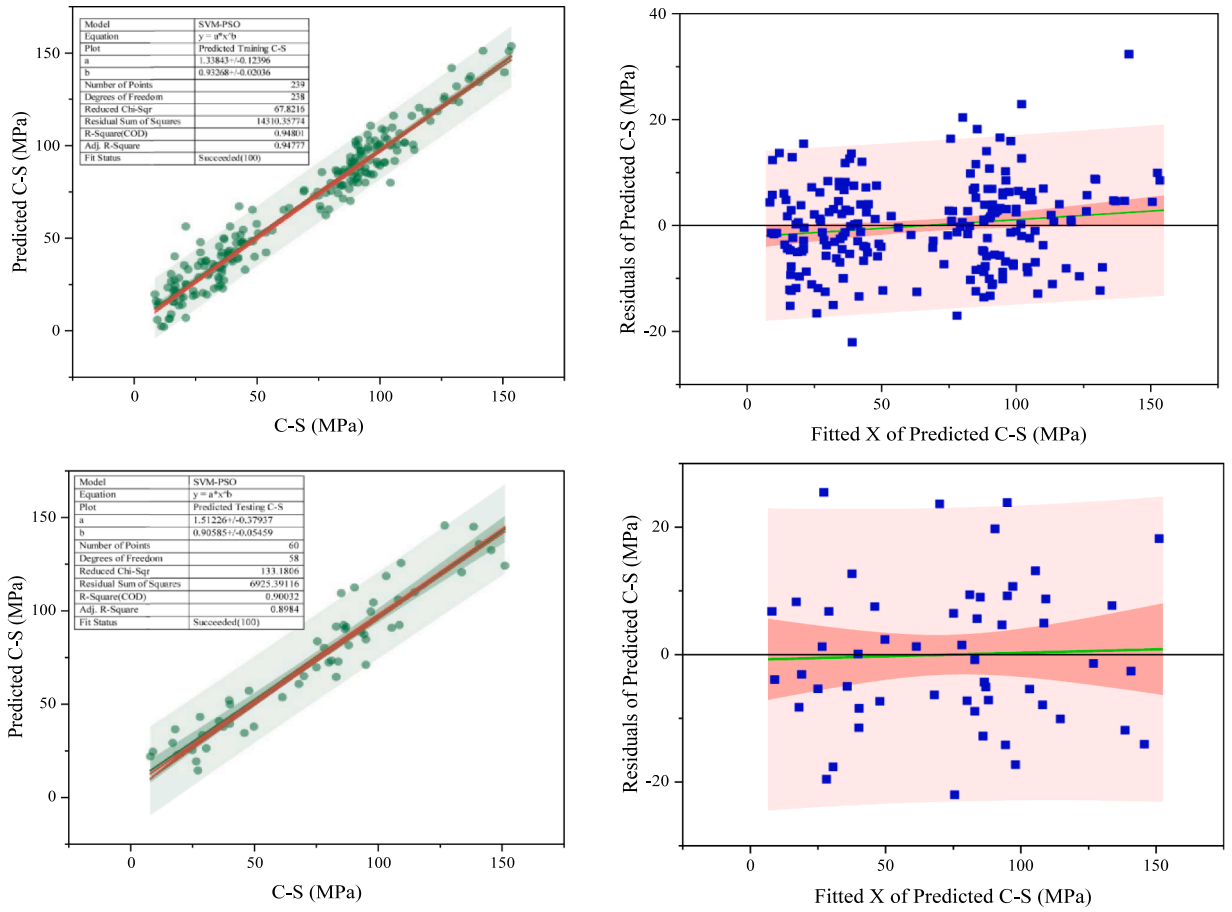

Fig. 16. The actual, predicted, and residual C-S of 3D-printed fiber-reinforced concrete with SVM-PSO model.

Table 9
The Analysis of variance (ANOVA) on the performance of a hybrid SVM-PSO model in predicting the compressive strength of 3D-printed concrete.

SVM-PSO Training						
		DF	SOS	M.S	F Value	Prob>F
Predicted Training C-S	Model	1	261228.3	261228.3	3923	2.72E−138
Predicted Training C-S	Error	211	14050.07	66.59		
Predicted Training C-S	Total	212	275278.3			
Fitted Y	Model	1	266439.9	266439.9	639317.1	0
Fitted Y	Error	211	87.94	0.42		
Fitted Y	Total	212	266527.9			
SVM-PSO Testing						
		DF	SOS	M.S	F Value	Prob>F
Predicted Testing C-S	Model	1	62745.6	62745.6	484.89	5.04E−28
Predicted Testing C-S	Error	52	6728.8	129.4		
Predicted Testing C-S	Total	53	69474.45			
Fitted Y	Model	1	65323	65323	63605.46	5.73E−82
Fitted Y	Error	52	53.41	1.03		
Fitted Y	Total	53	65376.41			

4.5. Taylor diagram of ML models

Taylor diagrams are used to evaluate machine learning models [112]. ML models for compressive strength of 3D-printed fiber-reinforced concrete are shown in the Taylor diagram in Fig. 20. Correlation, RMSE, and SD are used to evaluate dataset performance. Hybrid models based on the Particle Swarm Optimization (PSO) algorithm outperformed SVM, XGBoost, and RA in the Taylor curve performance study. In the training phase, these models showed high correlation coefficients exceeding 0.99, indicating their ability to relate real and anticipated concrete compressive strength values. These models performed well during testing. The

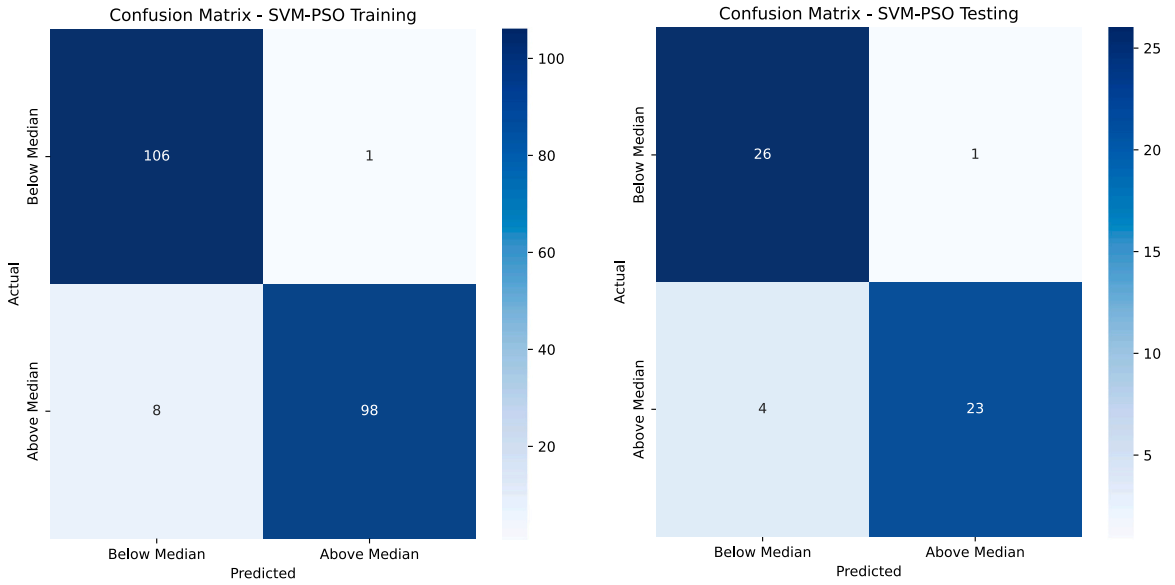

Fig. 17. The confusion matrix results of the SVM-PSO model for the training and testing phases.

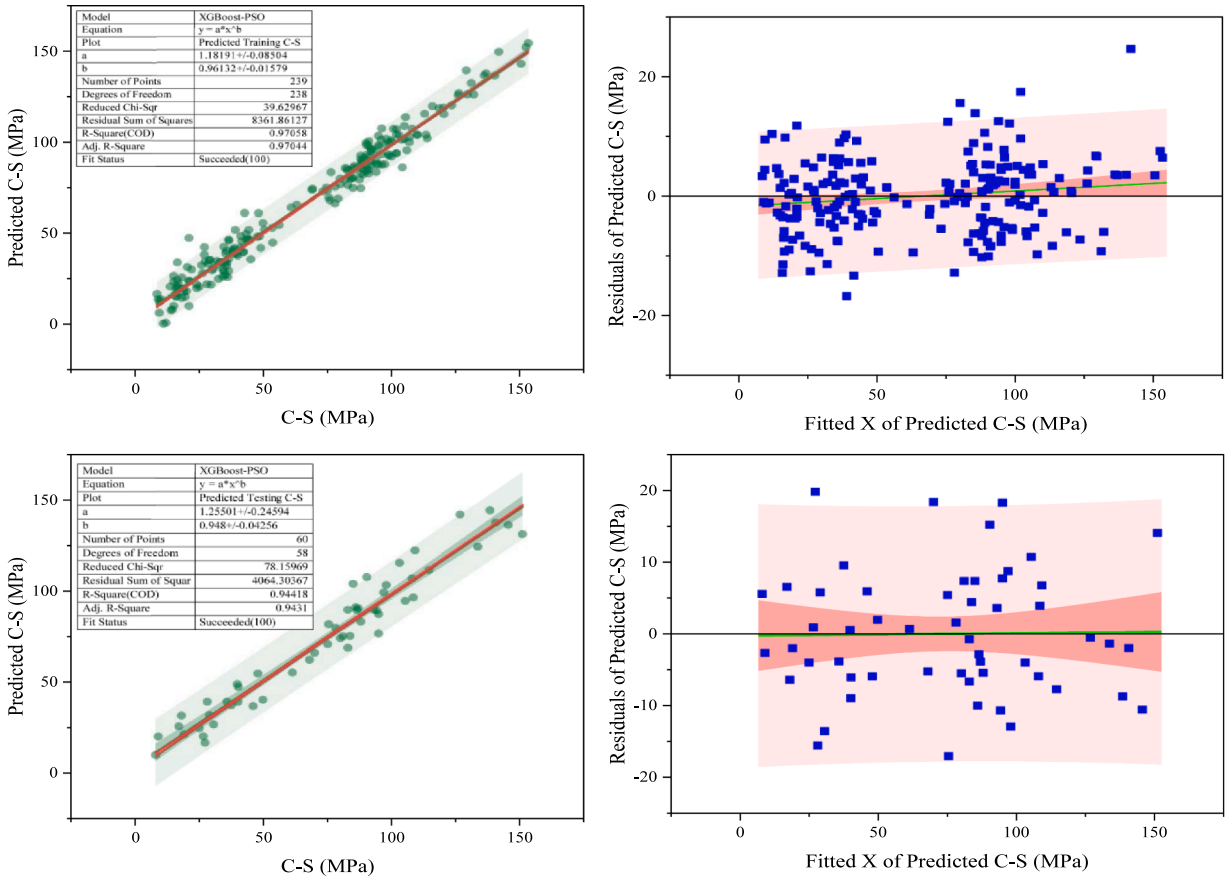

Fig. 18. The actual, predicted, and residuals of C-S of 3D-printed fiber-reinforced concrete with XGBoost-PSO model.

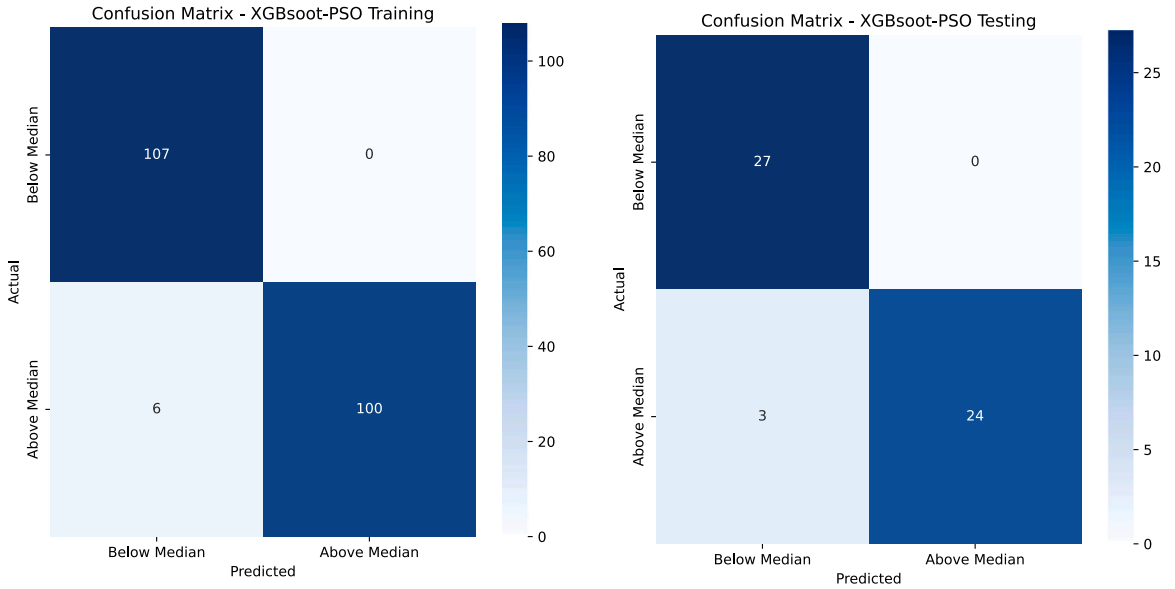

Fig. 19. The confusion matrix results of the SVM-PSO model for the training and testing phases.

Table 10
The Analysis of variance (ANOVA) on the performance of a hybrid XGBoost-PSO model in predicting the compressive strength of 3D-printed concrete.

XGBoost-PSO Training						
		DF	SOS	M.S	F Value	Prob>F
Predicted Training C-S	Model	1	275976	275976	7044.89	4.51E−164
Predicted Training C-S	Error	211	8265.69	39.18		
Predicted Training C-S	Total	212	284241.7			
Fitted Y	Model	1	279439.8	279439.8	1948270	0
Fitted Y	Error	211	30.27	0.14343		
Fitted Y	Total	212	279470			
XGBoost-PSO Testing						
		DF	SOS	M.S	F Value	Prob>F
Predicted Testing C-S	Model	1	68789.9	68789.9	890.516	2.18E−34
Predicted Testing C-S	Error	52	4016.86	77.25		
Predicted Testing C-S	Total	53	72806.75			
Fitted Y	Model	1	70117.11	70117.11	210995.4	1.68E−95
Fitted Y	Error	52	17.29	0.34		
Fitted Y	Total	53	70134.39			

SVM-PSO and RA-PSO models have correlation coefficients of 0.995 and standard deviations close to the actual data values, demonstrating their stability and efficiency in generalizing to unknown data [113]. However, the XGBoost-PSO model also performed well, with correlation coefficients exceeding 0.98 in the testing phase and a remarkable agreement in the standard deviation value compared to the actual values, indicating its robustness in predicting concrete properties, particularly compressive strength. With a correlation coefficient of 0.95, the CNN-LSTM model performed well [114]. However, its standard deviation exceeded that of the other models, indicating a modest difference between predicted and actual values. This difference may be attributed to the model's sensitivity to data temporality or input preprocessing [115].

The Taylor diagram in Fig. 20 illustrates the correlation, standard deviation, and centered root-mean-square difference between predicted and observed values for all models. The RA-PSO model shows the highest correlation and lowest RMSE, positioned closest to the reference point, indicating superior predictive accuracy and consistency compared to the other models.

4.6. Sensitivity analysis of ML models

Machine learning models need sensitivity analysis to determine input-output relationships[116]. It helps identify key components, explain nonlinear interactions, improve experimental design, and assess model reliability[117]. Due to the complexity of OPC, fiber type, W/B ratio, printing conditions like speed and temperature, and complex interactions, this analysis is essential for studying 3D-printed fiber-reinforced concrete compressive strength (CS). This field uses numerous sensitivity analysis methodologies, including the One-at-a-Time (OAT) method, which modifies one variable while holding all others constant. OAT quickly identifies sensitive

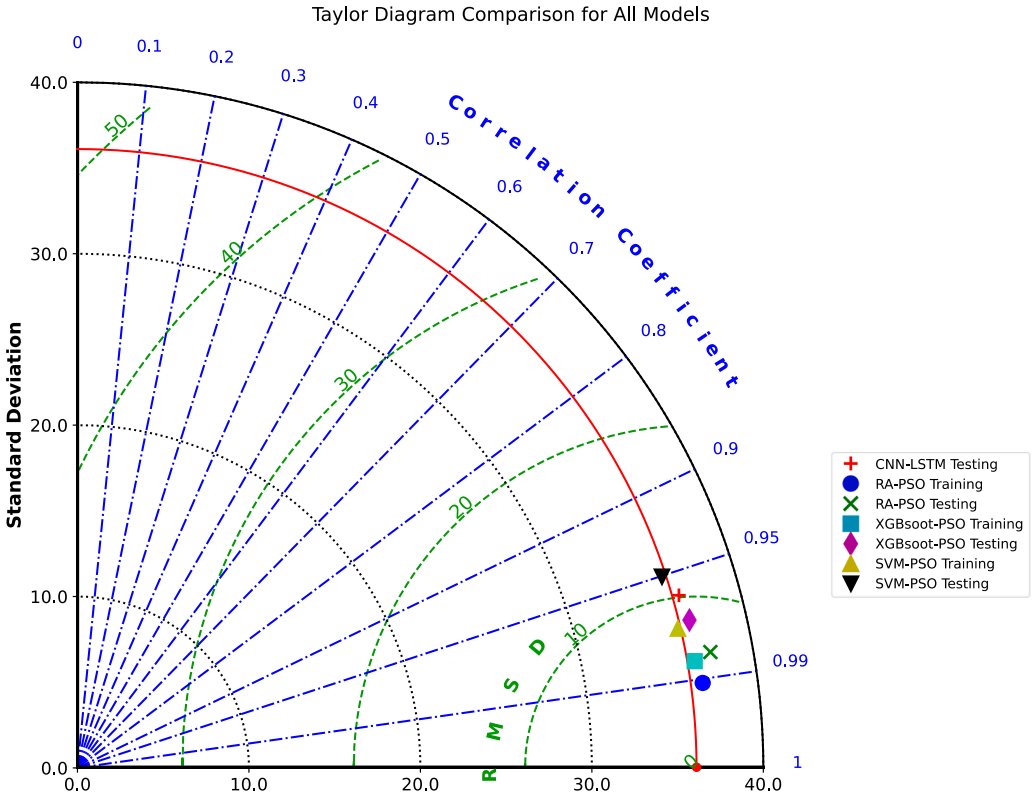

Fig. 20. Taylor diagrams of ML models for compressive strength of 3D-printed fiber-reinforced concrete.

variables and is simple to implement. However, it does not discover variable interactions and may misinterpret nonlinear relationships [118]. Probabilistic Bayesian optimization methods rapidly search the variable space, capturing complex variable interactions and decreasing testing, making them excellent for low-cost mixture parameter optimization to boost compressive strength. Fig. 21 shows the importance of the feature based on OOB. Out-of-bag (OOB) feature Importance analysis indicates that different factors affect model performance differently.

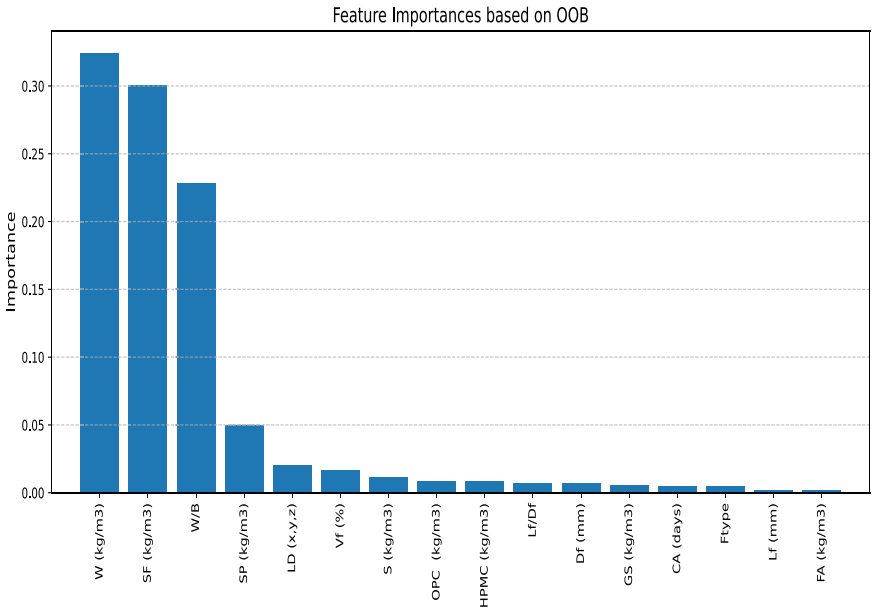

Fig. 21. The feature importances based on OOB.

Water (kg/m3) is the most important component in forecasting, at 34 %, followed by silica fume (kg/m3) at 30 %, and then W/B at 23 %. Factors like SP and LD (x,y,z) contribute 2.5–5 %, followed by geometric parameters like length (L) and fiber diameter (Df), which contribute 10 %. Some features, such as VF, sand (S), and OPC, have a less than 2.5 % impact and may be excluded to simplify the model without affecting accuracy [118]. The examination of model accuracy indicates that the error rate begins at 0.038 with 10 trees and progressively decreases to a minimum of 0.0275 with 140 trees, signifying a 27.6 % enhancement in accuracy. The model attains a plateau at 140 trees, and augmenting the quantity beyond this threshold does not yield a substantial enhancement in performance, as shown in Fig. 22. The optimal number of trees is 140 trees, which achieves the lowest OOB error value, indicating that the model has reached the highest possible accuracy before it starts to saturate or lose generalization efficiency [116]. Fig. 23 shows how each hyperparameter affects the optimization target, usually accuracy or error reduction. Partial dependence curves show how performance changes when one parameter changes while the others remain constant. The model's max_depth parameter, which reflects tree depth, shows that performance rises dramatically with depth. The deep tree represented data best at about 18, suggesting its best performance. The max_features option, which defines the proportion of features used in each tree, performed best near 0.45. Beyond this point, performance declined, suggesting that too many features could complicate the model. The model performed best with a low min samples leaf parameter, about 1.6. This shows that leaving with few samples helps the model respond to data better [119]. The highest performance was achieved at a low value, about 3, for the min samples split parameter, which defines the least number of samples needed to split the tree internally. Performance decreased as this number grew [120]. Model improvement was affected by the forest's tree count, n_estimators. Performance peaked at 160 trees, indicating that more trees produce more accurate and reliable forecasts. Fig. 24 shows the optimization algorithm focused extensively on values that showed promising performance at the beginning of the experiments, such as n_estimators = 160, max_depth = 18, and max_features ≈ 0.45, as well as small valuesof min_samples_leaf = 1.6 and min_samples_split = 3, reflecting the model's preference for flexibility in learning. Based on this, the best set of parameters was determined to be: max_depth = 18, max_features = 0.45, min_samples_leaf = 1.6, min_samples_split = 3, and n_estimators = 160. These sensitivity analysis results have direct implications for sustainable mix design in marine and civil infrastructure applications. In coastal environments, controlling the water-to-binder ratio is critical to minimizing permeability and chloride ingress, which directly improves durability against reinforcement corrosion. The identified significance of silica fume highlights its role in refining the pore structure and enhancing sulfate resistance, benefits that are particularly valuable in aggressive marine exposures. Optimizing water content, while maintaining workability, can reduce both shrinkage and the embodied carbon of the mix by minimizing excess cement paste. Integrating these parameter insights into the design phase allows engineers to select mix proportions that achieve the required mechanical performance while enhancing durability and reducing environmental impact, thus aligning with performance-based and sustainability-driven design objectives.

4.7. Prediction of CO_2 emissions

Given the global trend towards sustainable construction and climate change, precise carbon emission predictions for current building materials, such as 3D-printed fiber-reinforced concrete, are essential [121]. This technology revolutionizes building with its precise material distribution and minimized waste. Due to its numerous components and production methods, measuring its carbon

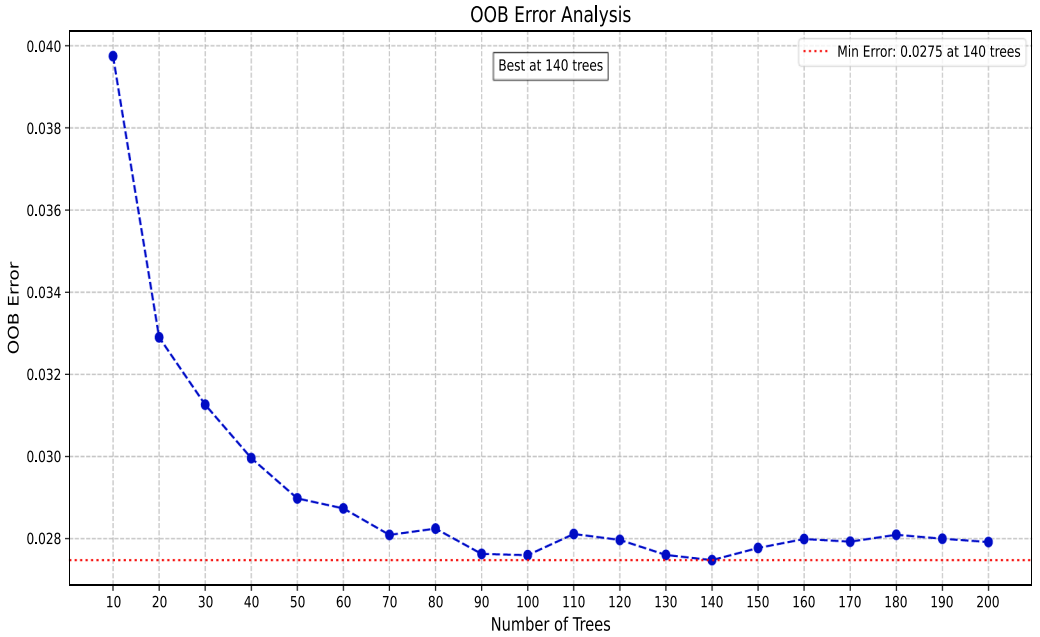

Fig. 22. The OOB error analysis.

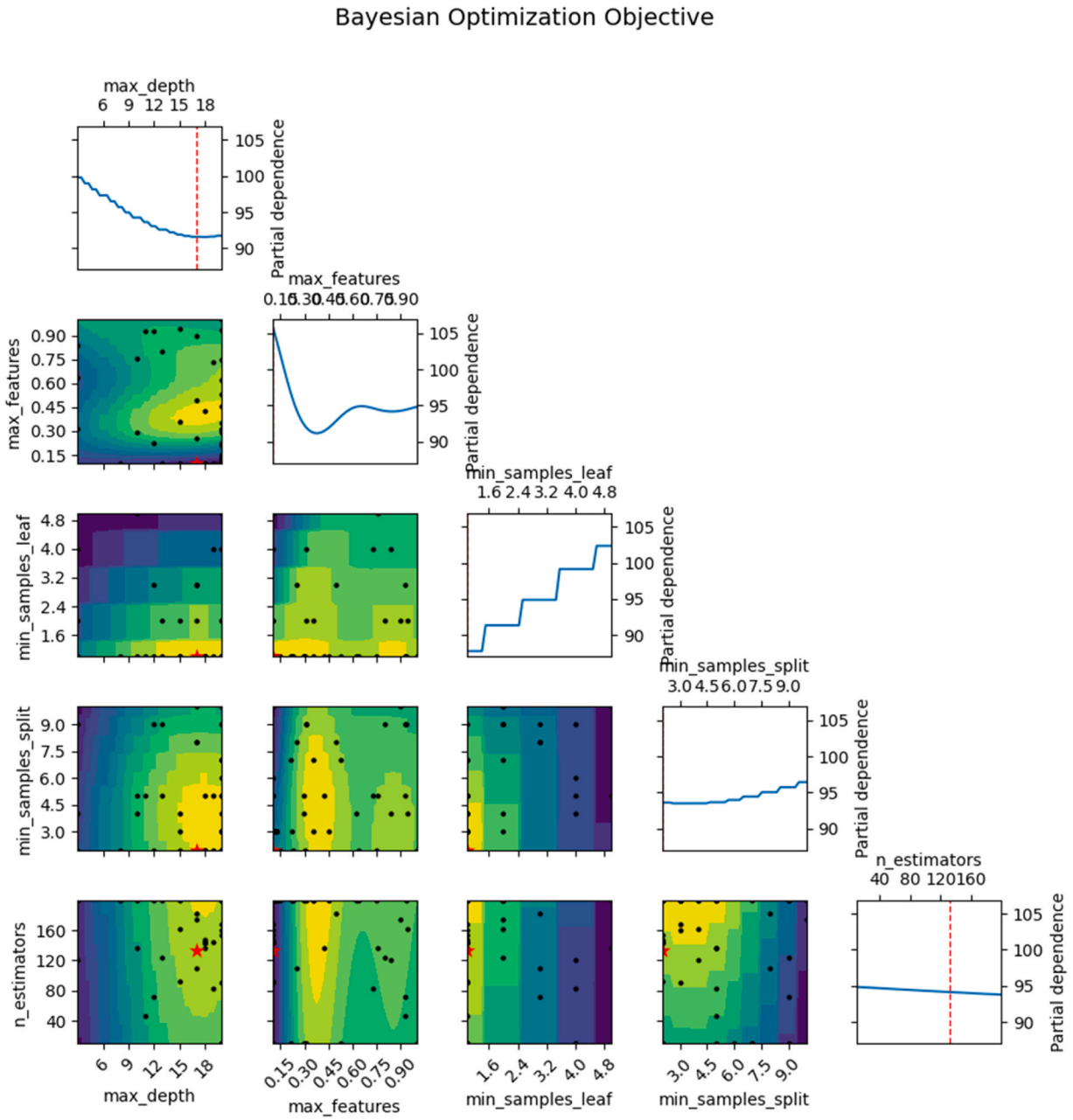

Fig. 23. The Bayesian optimization objective.

impact is difficult [122]. This work develops a quantitative predictive model by analyzing the association between manufacturing variables (e.g., printing speed, mix density, fiber ratio, and additive type) and CO_2 emissions [123]. This model uses machine learning and precise experimental data. The carbon footprint of 3D-printed fiber-reinforced concrete is evaluated in this section. RA-PSO, XGBoost-PSO, SVM-PSO and CNN-LSTM assess the carbon footprint, which includes total carbon dioxide emissions from the extraction of resources, processing, transportation, and production. The CO_2 emissions associated with each mix were initially calculated through conventional means, using the detailed mix proportions and established emission factors as presented in Table 11. These values represent the baseline, obtained through direct calculation from known quantities of each constituent material. However, these manually calculated values were not an end in themselves, they were subsequently used as target outputs for training the proposed machine learning models. The rationale for employing machine learning in this context is threefold. First, in many practical scenarios, especially during the early design phases of a project or when dealing with proprietary industrial formulations, the complete mix proportions may not be available to the designer or decision-maker. In such cases, only partial or indirect variables may be known, such as binder type, fiber characteristics, printing parameters, or early-age strength results. The trained ML models can leverage these

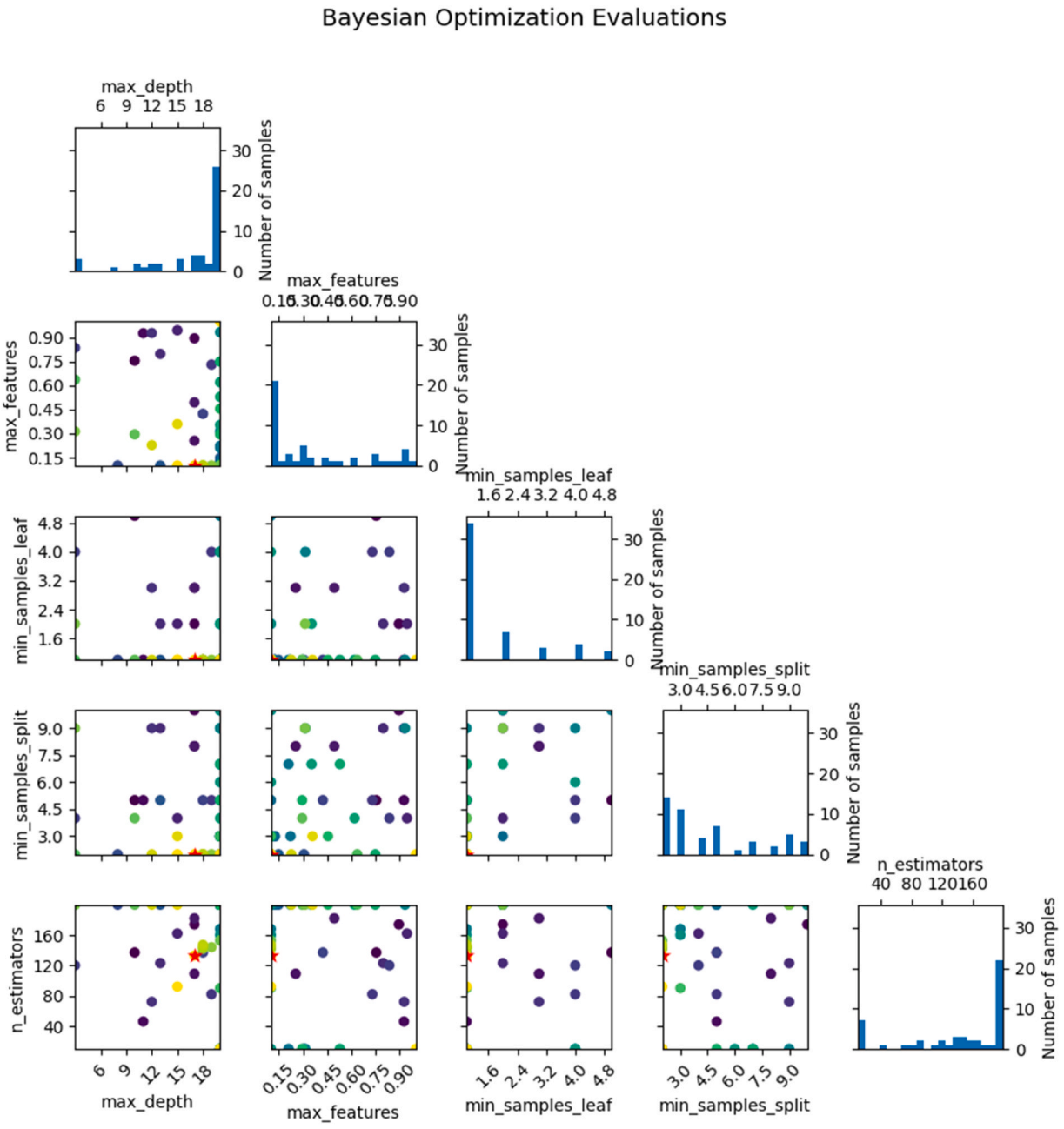

Fig. 24. The Bayesian optimization evaluations.

Table 11
CO_2 emissions from concrete raw materials.

Material	CO_2 Emissions (kg CO_2/kg material)	Ref.
OPC (kg/ m^3)	0.85	[35]
Sand (kg/ m^3)	0.01	
Fly Ash (kg/ m^3)	0.03	
Ground Slag (kg/m^3)	0.07	[124]
Silica Fume (kg/ m^3)	0.2	[35]
Super Plasticizer (kg/ m^3)	1.2	
Hydroxypropyl Methylcellulose (HPMC)	1.2	[125]
water (kg/m3)	0	

partial inputs to reliably estimate CO_2 emissions, filling a critical data gap that traditional calculation methods cannot address.

Second, integrating carbon emissions prediction into the same ML framework used for mechanical strength forecasting enables a multi-objective optimization process. Rather than treating strength and sustainability as separate evaluation steps, the proposed framework allows for simultaneous optimization of both parameters, leading to mix designs that balance performance with environmental impact. This integrated approach streamlines the decision-making process and facilitates trade-off analysis in real time. Third, the application of ML to emissions estimation provides a robust, data-driven alternative that can adapt and improve as more empirical datasets become available, including site-specific emission factors or regional supply chain data. This adaptability ensures that the predictions remain relevant across diverse geographical and industrial contexts. Table 11 presents the carbon footprints of the individual components used in the 3D-printed fiber-reinforced concrete mixes, derived from inventory data available in the literature. These values formed the foundation for the model training process, bridging the gap between traditional calculation methods and the advanced predictive capabilities demonstrated in this study.

In Fig. 25, four models are compared for their ability to estimate CO_2 emissions by analyzing the disagreement between actual and predicted values. RA-PSO, CNN-LSTM, XGBoost-PSO, and SVM-PSO are the models. The models were assessed using R^2 coefficients for training and test data and data dispersion around the ideal prediction line and 10 % uncertainty line. The best model was the RA-PSO, with a coefficient of determination of 0.97 on training data and 0.94 on testing data. Its strong performance shows that the model accurately represents variable relationships during training and generalizes fresh data well. The modest discrepancy between training and testing results, 0.03, demonstrates that the model is not overfitted, improving its dependability. The graph shows that most predicted sites are within ±10 % uncertainty, indicating great accuracy and closeness to reality. With a coefficient of determination of 0.95 for training and 0.92 for testing, the CNN-LSTM model performed well but badly compared to RA-PSO. Convolutional neural networks linked to long-term memory units are powerful architectures for processing time series and sequential data. Yet, this model performed 2.06 % worse in training and 2.13 % lower in testing than RA-PSO. Observations beyond the ±10 % uncertainty range suggest potential forecast accuracy issues, particularly in severe circumstances. After RA-PSO, XGBoost-PSO performed second with a coefficient of determination of 0.965 for training and 0.921 for testing. This performance strikes an excellent balance between learning and generalization, dropping 0.52 % in training and 2.02 % in testing compared to RA-PSO. Scores were near the ideal line with little variations, proving the model's stability and accuracy. For complex, multi-characteristic data, this model is highly trustworthy. The SVM-PSO model was the least accurate of the four, with training and testing coefficients of determination of 0.945 and 0.917. This performance decline indicates that the model was less resilient at learning or predicting than others. A difference of 0.028 between

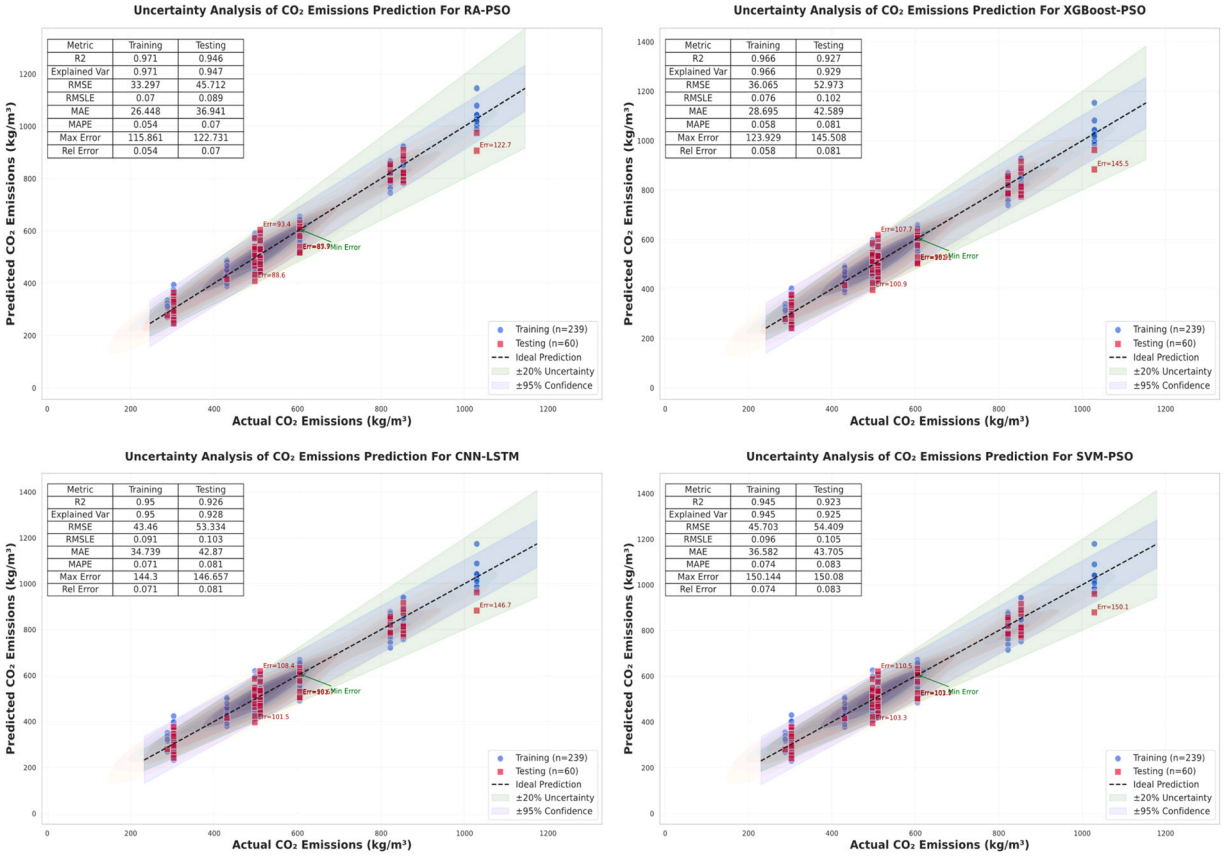

Fig. 25. Actual and predicted carbon dioxide (CO_2) emissions of concrete by RA-PSO, CNN-LSTM, XGBoost-PSO, and SVM-PSO.

training and testing is comparable to RA-PSO, although R2R2 has lower absolute values, indicating lesser accuracy overall. The prediction scores are also dispersed, suggesting that the model may be more error-prone or have not fully addressed all input data features. We found that the RA-PSO model outperformed the SVM-PSO model by 2.58 % on training data and 2.45 % on testing data. It beat the CNN-LSTM model by 2.06 % in training and 2.13 % in testing. It outperformed the XGBoost-PSO model by 0.52 % on training data and 2.02 % on testing data.

4.8. Graphical user interface (GUI) of 3D-printed fiber-reinforced concrete

The developed GUI streamlines complex software and hardware procedures in fiber-reinforced concrete 3D printing systems[126]. Without requiring any programming skills, it allows users to configure the printer, select the fiber type and mixing ratio, and set the print speed through intuitive visual windows and guided instructions[127]. The interface enables precise control of print paths and fiber orientation within layers, enhancing structural performance and strength. In real time, the GUI monitors key printing variables such as temperature, material flow, and layer stability, allowing immediate intervention in case of faults or deviations from the plan [128]. This accessibility makes the system suitable for non-experts; after brief training, engineers and technicians can operate it efficiently, reducing reliance on programming specialists and accelerating production[129]. Furthermore, the GUI can be integrated with sensors, augmented reality, and AI-based tools to further enhance automation and intelligence. Fig. 26**(a)** presents the GUI layouts for the RA-PSO, CNN-LSTM, XGBoost-PSO, and SVM-PSO models used to predict the compressive strength of 3DPFRC. Whereas the GUI layout for these to predict the CO_2 emissions of 3D-printed fiber-reinforced concrete is presented in Fig. 26**(b)**. The R^2 values for compressive strength prediction were 0.994, 0.979, 0.986, and 0.912 for RA-PSO, CNN-LSTM, XGBoost-PSO, and SVM-PSO, respectively, while for CO_2 emissions prediction, the R^2 values were 0.993, 0.936, 0.945, and 0.926.

5. Discussion

This study uses data from a decade of 3D-printed fiber-reinforced concrete research [1]. Using expert judgment, the results have been standardized despite variances in testing systems (e.g., testing time, experimental method, equipment condition, testing environment, and potential human errors) [130]. This study does not quantify data noise and uncertainty because they are not its main emphasis. Utilizing the dataset, we created a predictive ensemble model to assess the CO_2 emissions and compressive strength of several designs of 3DPFRC mixes [131]. These models integrate many algorithms (RA, SVM, and XGBoost) with PSO and additionally use CNN with LSTM, leveraging the strengths of each to predict 3D-printed fiber-reinforced concrete properties with balanced accuracy and generalizability. Using 3DPFRC signifies a notable progression in sustainable construction technology [132]. This work utilized four distinct predictive methodologies to estimate the CO_2 emissions linked to 3DPFRC production: RA-PSO, CNN-LSTM, SVM-PSO, and XGBoost-PSO. Each method offered significant insights into the environmental implications of this novel material, emphasizing both the advantages and constraints of each model [133]. Upon comparing the results from all four models, it is evident that machine learning methodologies, especially RA-PSO, provide promising instruments for sustainability evaluation in concrete additive manufacturing [43]. Nonetheless, the precision of predictions is significantly contingent upon the quality and quantity of data. Furthermore, the interpretability of results is a critical factor in model selection, particularly in contexts where transparency and traceability of decision-making are paramount [134]. Table 12 shows the decrease of R^2 (CO_2 emissions) for all models compared with RA-PSO.

This result of CO_2 emissions was lower than the carbon dioxide emission from 3D-printed fiber-reinforced concrete research in

Fig. 26. GUI of RA-PSO, CNN-LSTM, XGBoost-PSO, and SVM-PSO to predicted (a) C-S (b) CO_2 emissions.

many previous studies. Table 13 shows the carbon dioxide (CO_2) emissions for 1 m^3 for this study and previous Studies.

This study achieved a maximum carbon dioxide emission of 1029.5 kg/m^3 for 3D-printed fiber-reinforced concrete and predicted values with 1021.4, 1011.1,1035.2 and 1052.32 kg/m^3 for RA-PSO, CNN-LSTM, XGBoost-PSO, and SVM-PSO, respectively while the minimum carbon dioxide emission of 287.621 kg/m3 for 3D-printed fiber-reinforced concrete and predicted values with 280.12, 274.25,270.32 and 268.34 kg/m^3 for RA-PSO, CNN-LSTM, XGBoost-PSO, and SVM-PSO, respectively. Table 14 juxtaposes the existing models with those established in the literature for the compressive strength of 3D-printed concrete. Fig. 27 show the benefits of machine learning for 3D-printed fiber-reinforced concrete.

Beyond numerical performance metrics, the findings of this study demonstrate clear and actionable relevance to real-world engineering practice, particularly in the context of marine and civil infrastructure. The proposed machine learning models, especially the RA-PSO framework, offer more than theoretical accuracy; they provide a practical decision-support tool that can be directly embedded into the material design and planning stages of construction projects. In marine environments, structures such as quay walls, breakwaters, and offshore platforms are routinely exposed to aggressive agents, including chlorides, sulfates, and cyclic wetting-drying conditions. The accurate prediction of compressive strength enables engineers to tailor 3D-printed fiber-reinforced concrete mixes with enhanced resistance to chloride ingress and sulfate-induced deterioration. By integrating such predictive capabilities early in the design process, the service life of these structures can be significantly prolonged, reducing the frequency and cost of repairs.

Equally critical is the model's ability to forecast CO_2 emissions for different mix configurations. This feature directly supports the adoption of low-carbon concrete alternatives without compromising mechanical performance. In civil infrastructure projects such as bridges, retaining walls, or coastal flood defense systems, decision-makers can use these predictions to evaluate multiple design scenarios, balancing structural safety with environmental sustainability. For example, in the design of a marine quay wall, the RA-PSO model can identify optimal material proportions that meet the required strength while cutting embodied CO_2 emissions by up to 50 % compared to conventional cement-rich designs. The integration of such predictive models into design workflows promotes a comprehensive approach to infrastructure planning; one that simultaneously enhances durability, ensures compliance with environmental regulations, and minimizes lifecycle costs. Ultimately, these findings bridge the gap between advanced machine learning research and its tangible benefits for sustainable, long-lasting, and cost-effective marine and civil engineering applications.

6. Conclusion

This study developed reliable hybrid machine learning models (RA-PSO, CNN-LSTM, XGBoost-PSO, SVM-PSO) to predict compressive strength and CO_2 emissions of 3D-printed fiber-reinforced concrete (3DPFRC) for sustainable marine and civil infrastructure. Using 16 input variables, the models demonstrated high generalizability and accuracy, as validated by metrics such as R^2, MSE, AIC, BIC, precision, recall, and F1 score. Sensitivity analysis and Bayesian optimization revealed influential mix parameters. The results confirm the models' potential to guide the design of low-carbon, high-performance marine structures, such as revetments, precast docks, and offshore components. Following conclusions are made:

1. Four hybrid models (RA-PSO, CNN-LSTM, XGBoost-PSO, SVM-PSO) were evaluated for predicting compressive strength and CO_2 emissions of 3DPFRC, all achieving $R^2 > 0.9$.
2. The RA-PSO model demonstrated the best overall performance in both training and testing phases for both targets.
3. Overall statistical ranking was: RA-PSO < XGBoost-PSO < CNN-LSTM < SVM-PSO.
4. After hyperparameter optimization, the OOB error decreased from 0.038 to 0.0275, representing a 27.6 % improvement.
5. Sensitivity analysis identified water content (34 %), silica fume (30 %), and water-to-binder ratio (23 %) as the most influential features, while sand, OPC, and fiber volume had negligible impacts (<2.5 %).
6. RA-PSO achieved $R^2 = 0.94$ for CO_2 emissions prediction in testing, with most estimates within ±10 % uncertainty.
7. The developed GUI enabled real-time control and monitoring without programming, achieving high prediction accuracy ($R^2 = 0.994$ for compressive strength and $R^2 = 0.993$ for CO_2 emissions).
8. Taylor diagram analysis confirmed the superiority of PSO-based hybrid models, especially RA-PSO and SVM-PSO, with correlation coefficients up to 0.995 and standard deviations closely matching actual data.

Future research should incorporate more 3D printing factors in a comprehensive experimental database, including printing speed, ambient temperature, and early-age setting time. Smart sensing and interactive AI could improve print quality monitoring and real-time control. Ultimately, more interpretable hybrid models that combine high accuracy with simplicity of understanding are needed to deploy these models in large-scale industrial and technical applications for Sustainable Marine and Civil Infrastructure.

Table 12
The decrease of R^2 for all models compared with RA-PSO.

Model	R^2 train	R^2 test	Difference from RA-PSO (train)	Difference from RA-PSO (test)
RA-PSO	0.97	0.94	–	–
CNN-LSTM	0.95	0.92	−2.06 %	−2.13 %
XGBoost-PSO	0.965	0.921	−0.52 %	−2.02 %
SVM-PSO	0.945	0.917	−2.58 %	−2.45 %

Table 13
The carbon dioxide (CO_2) emissions for 1 m^3 for this study and previous Studies.

Ref.	[135]	[136]	[137]	this study
CO_2 emissions / 1 m^3	330	508	650	287.621

Table 14
Comparison of the established models with literature models.

Model	R^2	MAE	RMSE	Ref.
ANN	0.96	11.2	7.9	[138]
NGBoost	0.96	11.4	8.1	[1]
MEP	0.95	11.9	8.6	
RF	0.92	12.1	8.8	
SVM	0.92	12.3	9	
XGBoost	0.85	13.5	10.2	[139]
RF	0.83	14.1	10.8	[140]
SVR	0.71	16.8	13.5	
MLR	0.42	6.3	18	[141]
This study	0.98	5.819	6.944	

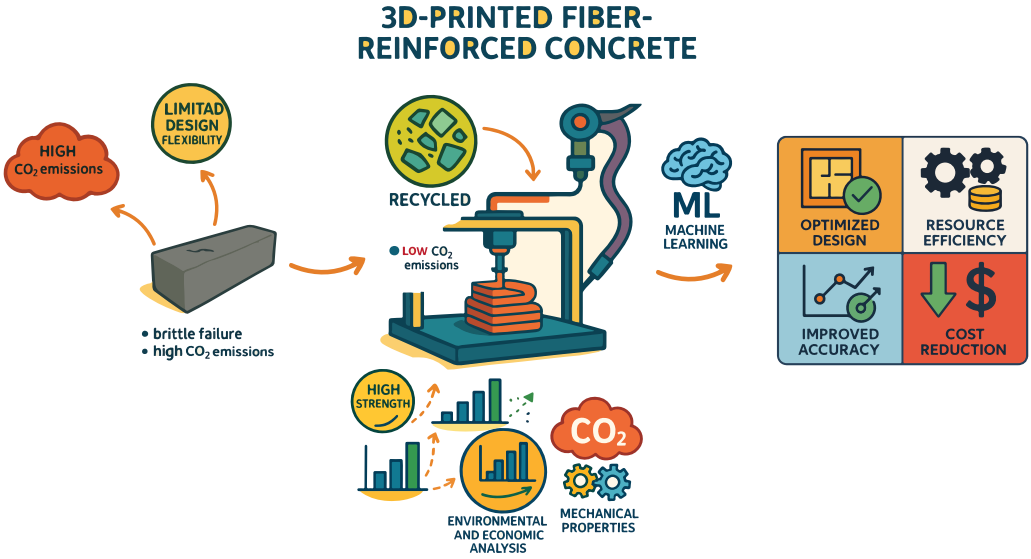

Fig. 27. The Benefits of machine learning for 3D-printed fiber-reinforced concrete.

CRediT authorship contribution statement

Ahmed A. Abdou Elabbasy: Writing – review & editing, Methodology, Investigation, Data curation. **Nasser Alanazi:** Writing – review & editing, Validation, Resources, Methodology. **Tong Liu:** Writing – original draft, Software, Resources, Methodology. **Muwaffaq Alqurashi:** Writing – review & editing, Visualization, Investigation, Funding acquisition. **Pshtiwan Shakor:** Writing – review & editing, Supervision, Resources. **Shijie Liu:** Writing – original draft, Methodology, Conceptualization.

Declaration of Competing Interest

The authors declare no conflict of interest.

Acknowledgment

This work was supported by Key research and development project for introducing high-level scientific and technological talents in Lyliang City (2022RC23); Scientific and Technological Innovation Programs of Higher Education Institutions in Shanxi (2022L566); 2024 Shanxi Province College Students Innovation and Entrepreneurship Training Program Project (20241308); Lyuliang University Special Fund for Young Academic Backbones (03013030004). The authors extend their appreciation to Taif University, Saudi Arabia, for supporting this work through project number (TU-DSPP-2024–248).

Data availability

Data will be made available on request.

References

[1] M.N. Uddin, J. Ye, B. Deng, L.-z Li, K. Yu, Interpretable machine learning for predicting the strength of 3D printed fiber-reinforced concrete (3DP-FRC), J. Build. Eng. 72 (2023) 106648.
[2] R.I. Rasel, M.M. Hossain, M.H. Zubayer, C. Zhang, Exploring the fresh and rheology properties of 3D printed concrete with fiber reinforced composites (3DP-FRC): a novel approach using machine learning techniques, Mater. Res. Express 11 (12) (2024) 125502.
[3] W. Xu, D. Jiang, Q. Zhao, L. Wang, Study on printability of 3D printing carbon fiber reinforced eco-friendly concrete: characterized by fluidity and consistency, Case Stud. Constr. Mater. 21 (2024) e03589.
[4] W. Yang, L. Wang, Y. Hu, J. Sanjayan, G. Ma, An integrated topology optimization method including manufacturing constraints for 3D printed fiber-reinforced concrete structures, Mater. Lett. 355 (2024) 135442.
[5] L. Casagrande, 3D Concr. Print. a N. Era Constr. Ind. (2020).
[6] M.N. Uddin, J. Ye, M.A. Haque, K. Yu, L. Li, A novel compressive strength estimation approach for 3D printed fiber-reinforced concrete: integrating machine learning and gene expression programming, Multiscale Multidiscip. Model. Exp. Des. 7 (5) (2024) 4889–4910.
[7] A. Ahmed, M.N. Uddin, M. Akbar, R. Salih, M.A. Khan, H. Bisheh, T. Rabczuk, Prediction of shear behavior of glass FRP bars-reinforced ultra-highperformance concrete I-shaped beams using machine learning, Int. J. Mech. Mater. Des. 20 (2) (2024) 269–290.
[8] P. Barve, A. Bahrami, S. Shah, Geopolymer 3D printing: a comprehensive review on rheological and structural performance assessment, printing process parameters, and microstructure, Front. Mater. 10 (2023) 1241869.
[9] J. Shi, X. Cao, H. Wang, Infrastructure-Oriented efficient materials implemented with fibers, Buildings 15 (4) (2025) 609.
[10] T.J. Brunjes, Crit. Eval. Constr. Ind. Relat. Addit. Manuf. Res. A Scientometr. Anal. (2022).
[11] P.D. Nguyen, M.B. Dao, T.Q. Nguyen, Hybrid supervised and Self-Supervised learning for 3D printing optimization: a masked supervised bootstrap your own latent approach, 3D Print. Addit. Manuf. (2025).
[12] P. Ni, F. Lei, H. Zheng, J. Song, Z. Zheng, G. Qin, and Z. Yan, Multi-Dimensional Coupled Evaluation and Prediction Of Solar Energy Utilization Indicators on Building Surfaces, Zhuoxin and Qin, Guojin and Yan, Zengfeng, Multi-Dimensional Coupled Evaluation and Prediction Of Solar Energy Utilization Indicators on Building Surfaces.
[13] J. Xiao, et al., Large-scale 3D printing concrete technology: current status and future opportunities, Cem. Concr. Compos. 122 (2021) 104115.
[14] M.A.H. Khan, et al., Comprehensive review of 3D printed concrete, life cycle assessment, AI and ML models: materials, engineered properties and techniques for additive manufacturing, Sustain. Mater. Technol. 43 (2025) e01164.
[15] X. Wang, W. Li, Y. Guo, A. Kashani, K. Wang, L. Ferrara, I. Agudelo, Concrete 3D printing technology in sustainable construction: a review on raw materials, concrete types and performances, Dev. Built Environ. (2024) 100378.
[16] F. Lyu, D. Zhao, X. Hou, L. Sun, Q. Zhang, Overview of the development of 3D-printing concrete: a review, Appl. Sci. 11 (21) (2021) 9822.
[17] R.A. Mohamed, A.F.A. Mohamed, Exploring the environmental benefits of 3D printing technology in concrete construction; a review, Prog. Addit. Manuf. 10 (1) (2025) 279–289.
[18] D. Liu, Z. Zhang, X. Zhang, Z. Chen, 3D printing concrete structures: state of the art, challenges, and opportunities, Constr. Build. Mater. 405 (2023) 133364.
[19] M. Khan, C. McNally, Recent developments on low carbon 3D printing concrete: revolutionizing construction through innovative technology, Clean. Mater. (2024) 100251.
[20] G. Ma, R. Buswell, W.R.L. da Silva, L. Wang, J. Xu, S.Z. Jones, Technology readiness: a global snapshot of 3D concrete printing and the frontiers for development, Cem. Concr. Res. 156 (2022) 106774.
[21] R. Fang, B. Wang, J. Pan, J. Liu, Z. Wang, Q. Wang, X. Ling, Effect of concrete surface roughness on shear strength of frozen soil–concrete interface based on 3D printing technology, Constr. Build. Mater. 366 (2023) 130158.
[22] D. Dey, D. Srinivas, B. Panda, P. Suraneni, T. Sitharam, Use of industrial waste materials for 3D printing of sustainable concrete: a review, J. Clean. Prod. 340 (2022) 130749.
[23] C.-H. Ko, Constraints and limitations of concrete 3D printing in architecture, J. Eng. Des. Technol. 20 (5) (2022) 1334–1348.
[24] N. Singh, F. Colangelo, I. Farina, Sustainable Non-Conventional concrete 3D Printing—A review, Sustainability 15 (13) (2023) 10121.
[25] Z. Zhao, C. Ji, J. Xiao, L. Yao, C. Lin, T. Ding, T. Ye, A critical review on reducing the environmental impact of 3D printing concrete: material preparation, construction process and structure level, Constr. Build. Mater. 409 (2023) 133887.
[26] S. Wan, C. Yan, Z. Liu, L. Liu, Prediction of bending strength in ECC-RC composite beams using machine learning-based models, Int. J. Struct. Integr. (2025).
[27] K. ABDALGADER, Machine learning approach for predicting the compressive and flexural strengths of fiber-reinforced concrete mixtures, Materials Research Proceedings, vol. 48.
[28] A. Kashem, R. Karim, P. Das, S.D. Datta, M. Alharthai, Compressive strength prediction of sustainable concrete incorporating rice husk ash (RHA) using hybrid machine learning algorithms and parametric analyses, Case Stud. Constr. Mater. 20 (2024) e03030.
[29] M. Mishra, Quantifying compressive strength in limestone powder incorporated concrete with incorporating various machine learning algorithms with SHAP analysis, Asian J. Civ. Eng. 26 (2) (2025) 731–746.
[30] M.F. Javed, M. Fawad, R. Lodhi, T. Najeh, Y. Gamil, Forecasting the strength of preplaced aggregate concrete using interpretable machine learning approaches, Sci. Rep. 14 (1) (2024) 8381.
[31] P. Zhang, F. Kong, H. Lu, Strength prediction of smart cementitious materials using a neural network optimized by particle swarm algorithm, Buildings 14 (7) (2024) 2033.
[32] V. Poluektova, M. Poluektov, Artificial intelligence in materials science and modern concrete technologies: analysis of possibilities and prospects, Inorg. Mater. Appl. Res. 15 (5) (2024) 1187–1198.
[33] X.-R. Ma, X.-L. Wang, S.-Z. Chen, Trustworthy machine learning-enhanced 3D concrete printing: predicting bond strength and designing reinforcement embedment length, Autom. Constr. 168 (2024) 105754.
[34] S. Hong, J. Wu, B. Dong, Y. Zhang, P. Wang, Performance evaluation of conductive materials in conductive mortar based on machine learning, J. Build. Eng. 92 (2024) 109695.
[35] A. Essam, S.A. Mostafa, M. Khan, A.M. Tahwia, Modified particle packing approach for optimizing waste marble powder as a cement substitute in high-performance concrete, Constr. Build. Mater. 409 (2023) 133845.
[36] P. Ni, F. Lei, H. Zheng, J. Song, Z. Zheng, Z. Yan, and G. Qin, Multi-Dimensional Coupled Evaluation and Prediction Of Solar Energy Utilization Indicators on Building Surfaces: A Case Study on Non-Enriched Area, China, Zengfeng and Qin, Guojin, Multi-Dimensional Coupled Evaluation and Prediction Of Solar Energy Utilization Indicators on Building Surfaces: A Case Study on Non-Enriched Area, China.
[37] J. Ukwaththa, S. Herath, D. Meddage, A review of machine learning (ML) and explainable artificial intelligence (XAI) methods in additive manufacturing (3D printing), Mater. Today Commun. (2024) 110294.
[38] F.M. Talaat, E. Hassan, Artificial intelligence in 3D printing. Enabling Machine Learning Applications in Data Science: Proceedings of Arab Conference for Emerging Technologies 2020, Springer, 2021, pp. 77–88.
[39] M. Rastak, S. Vanaei, S. Vanaei, M. Moezzibadi, Machine learning in 3D printing, Ind. Strateg. Solut. 3D Print. Appl. Optim. (2024) 273–294.
[40] S. Geng, Q. Luo, K. Liu, Y. Li, Y. Hou, W. Long, Research status and prospect of machine learning in construction 3D printing, Case Stud. Constr. Mater. 18 (2023) e01952.

[41] J.J. Ong, B.M. Castro, S. Gaisford, P. Cabalar, A.W. Basit, G. Pérez, A. Goyanes, Accelerating 3D printing of pharmaceutical products using machine learning, Int. J. Pharm. X 4 (2022) 100120.
[42] P.D. Nguyen, T.Q. Nguyen, Q. Tao, F. Vogel, H. Nguyen-Xuan, A data-driven machine learning approach for the 3D printing process optimisation, Virtual Phys. Prototyp. 17 (4) (2022) 768–786.
[43] M. Arif, et al., Data-driven models for predicting compressive strength of 3D-printed fiber-reinforced concrete using interpretable machine learning algorithms, Case Stud. Constr. Mater. 21 (2024) e03935.
[44] H. Wu, et al., Effects of binder component and curing regime on compressive strength, capillary water absorption, shrinkage and pore structure of geopolymer mortars, Constr. Build. Mater. 442 (2024) 137707.
[45] S. Zhang, X. Qi, S. Guo, L. Zhang, J. Ren, A systematic research on foamed concrete: the effects of foam content, Fly ash, slag, silica fume and water-to-binder ratio, Constr. Build. Mater. 339 (2022) 127683.
[46] O.Y. Mady, O. Dewedar, N. Abdine, H. Zaytoon, Y. Haggag, Bioadhesive behaviors of HPMC E5: comparative analysis of various techniques, histological and human radiological evidence, Sci. Rep. 14 (1) (2024) 1840.
[47] C. Wen, P. Zhang, J. Wang, S. Hu, Influence of fibers on the mechanical properties and durability of ultra-high-performance concrete: a review, J. Build. Eng. 52 (2022) 104370.
[48] H. Liang, L. Shi, D. Wang, X. Xiao, K. Deng, Influence of graded coarse aggregate content and specific surface area on the fracture properties of asphalt mixtures based on discrete element simulations and indoor tests, Constr. Build. Mater. 299 (2021) 123942.
[49] H. Ling, C. Qian, W. Kang, C. Liang, H. Chen, Combination of support vector machine and K-Fold cross validation to predict compressive strength of concrete in marine environment, Constr. Build. Mater. 206 (2019) 355–363.
[50] Z. Lyu, Y. Yu, B. Samali, M. Rashidi, M. Mohammadi, T.N. Nguyen, A. Nguyen, Back-propagation neural network optimized by K-fold cross-validation for prediction of torsional strength of reinforced concrete beam, Materials 15 (4) (2022) 1477.
[51] M.A. Khan, A. Zafar, F. Farooq, M.F. Javed, R. Alyousef, H. Alabduljabbar, M.I. Khan, Geopolymer concrete compressive strength via artificial neural network, adaptive neuro fuzzy interface system, and gene expression programming with K-fold cross validation, Front. Mater. 8 (2021) 621163.
[52] Y. Zhao, K. Zhang, A. Guo, F. Hao, J. Ma, Predictive model for erosion rate of concrete under wind gravel flow based on K-Fold Cross-Validation combined with support vector machine, Buildings 15 (4) (2025) 614.
[53] Y.S. Reddy, A. Sekar, S.S. Nachiar, Predictive analysis of foam concrete compressive strength: a comparative study of OLS and SVR with K-fold validation, Asian J. Civ. Eng. 25 (3) (2024) 2599–2608.
[54] D. Abriha, P.K. Srivastava, S. Szabó, Smaller is better? Unduly nice accuracy assessments in roof detection using remote sensing data with machine learning and k-fold cross-validation, Heliyon 9 (3) (2023).
[55] S. Singh, S.K. Patro, S.K. Parhi, Evolutionary optimization of machine learning algorithm hyperparameters for strength prediction of high-performance concrete, Asian J. Civ. Eng. 24 (8) (2023) 3121–3143.
[56] P.G. Asteris, A.D. Skentou, A. Bardhan, P. Samui, K. Pilakoutas, Predicting concrete compressive strength using hybrid ensembling of surrogate machine learning models, Cem. Concr. Res. 145 (2021) 106449.
[57] K. Güçlüer, A. Özbeyaz, S. Göymen, O. Günaydın, A comparative investigation using machine learning methods for concrete compressive strength estimation, Mater. Today Commun. 27 (2021) 102278.
[58] Z. Li, J. Yoon, R. Zhang, F. Rajabipour, W.V. Srubar III, I. Dabo, A. Radlińska, Machine learning in concrete science: applications, challenges, and best practices, npj Comput. Mater. 8 (1) (2022) 127.
[59] Y. Gamil, Machine learning in concrete technology: a review of current researches, trends, and applications, Front. Built Environ. 9 (2023) 1145591.
[60] P. Ziolkowski, M. Niedostatkiewicz, Machine learning techniques in concrete mix design, Materials 12 (8) (2019) 1256.
[61] H. Nguyen, T. Vu, T.P. Vo, H.-T. Thai, Efficient machine learning models for prediction of concrete strengths, Constr. Build. Mater. 266 (2021) 120950.
[62] M. Kumar, et al., A hybrid model based on convolution neural network and long short-term memory for qualitative assessment of permeable and porous concrete, Case Stud. Constr. Mater. 19 (2023) e02254.
[63] L. Ding, W. Fang, H. Luo, P.E. Love, B. Zhong, X. Ouyang, A deep hybrid learning model to detect unsafe behavior: integrating convolution neural networks and long short-term memory, Autom. Constr. 86 (2018) 118–124.
[64] H. Chen, X. Li, Y. Wu, L. Zuo, M. Lu, Y. Zhou, Compressive strength prediction of high-strength concrete using long short-term memory and machine learning algorithms, Buildings 12 (3) (2022) 302.
[65] B.A. Demiss, W.A. Elsaigh, Application of novel hybrid deep learning architectures combining convolutional neural networks (CNN) and recurrent neural networks (RNN): construction duration estimates prediction considering preconstruction uncertainties, Eng. Res. Express 6 (3) (2024) 032102.
[66] X. Zhang, et al., High-speed railway seismic response prediction using CNN-LSTM hybrid neural network, J. Civ. Struct. Health Monit. 14 (5) (2024) 1125–1139.
[67] O. Yazdanpanah, M. Chang, E.Ali Bakhshi, Attention-based hybrid convolutional-long short-term memory network for bridge pier hysteresis and backbone curves prediction, 10692509241301240, Integr. Comput. Aided Eng. (2024), 10692509241301240.
[68] J. Du, Y. Liu, Y. Yu, W. Yan, A prediction of precipitation data based on support vector machine and particle swarm optimization (PSO-SVM) algorithms, Algorithms 10 (2) (2017) 57.
[69] L.K. Alsaykhan, M.S. Maashi, A hybrid detection model for acute lymphocytic leukemia using support vector machine and particle swarm optimization (SVM-PSO), Sci. Rep. 14 (1) (2024) 23483.
[70] H. Zhao, A. Wei, F. Ma, F. Dai, Y. Jiang, H. Li, Comparison of debris flow susceptibility assessment methods: support vector machine, particle swarm optimization, and feature selection techniques, J. Mt. Sci. 21 (2) (2024) 397–412.
[71] E. Elsedimy, S.M. AboHashish, F. Algarni, New cardiovascular disease prediction approach using support vector machine and quantum-behaved particle swarm optimization, Multimed. Tools Appl. 83 (8) (2024) 23901–23928.
[72] R. Kuo, T.-H. Chiu, Hybrid of jellyfish and particle swarm optimization algorithm-based support vector machine for stock market trend prediction, Appl. Soft Comput. 154 (2024) 111394.
[73] M. Arif, F.U. Rehman, L. Sekanina, A.S. Malik, A comprehensive survey of evolutionary algorithms and metaheuristics in brain EEG-based applications, J. Neural Eng. (2024).
[74] I. Meir, A. Bechar, A. Sintov, Kinematic optimization of a robotic arm for automation tasks with human demonstration. 2024 IEEE International Conference on Robotics and Automation (ICRA), IEEE, 2024, pp. 7172–7178.
[75] M.N.A. Raja, T. Abdoun, W. El-Sekelly, Exploring the potential of machine learning in stochastic reliability modelling for reinforced soil foundations, Buildings 14 (4) (2024) 954.
[76] F. Salehi, et al., PRECISE-RA: predicting remission and StratifyingRisk in rheumatoid arthritis patients treated withbDMARDs—A, Robust. Mach. Learn. Approach (2025).
[77] P. Kumar, S. Shekhar Kamal, A. Kumar, N. Kumar, S. Kumar, Compressive strength of bentonite concrete using state-of-the-art optimised XGBoost models, Nondestruct. Test. Eval. (2024) 1–24.
[78] Utkarsh, P.K. Jain, Predicting bentonite swelling pressure: optimized XGBoost versus neural networks, Sci. Rep. 14 (1) (2024) 17533.
[79] M.H. Kadkhodaei, V. Amirkiyaei, E. Ghasemi, Developing two robust hybrid models for predicting tunnel deformation in squeezing prone grounds, Transp. Geotech. 45 (2024) 101231.
[80] M. Ghadamyari, Advancing Energy Forecasting: Integrating Data Mining and Hybrid Machine Learning Techniques for Enhanced Peak Load and Demand Prediction, Available at SSRN 4764479.
[81] A. Gebretsadik, et al., Enhancing rock fragmentation assessment in mine blasting through machine learning algorithms: a practical approach, Discov. Appl. Sci. 6 (5) (2024) 223.

[82] S. Rustad, M. Akrom, T. Sutojo, H.K. Dipojono, A feature restoration for machine learning on anti-corrosion materials, Case Stud. Chem. Environ. Eng. 10 (2024) 100902.
[83] S. Aggarwal, R. Singh, A. Rathore, K. Kapoor, M. Patel, A novel data-driven machine learning techniques to predict compressive strength of Fly ash and recycled coarse aggregates based self-compacting concrete, Mater. Today Commun. 39 (2024) 109294.
[84] N.-D. Hoang, Leveraging a hybrid machine learning approach for compressive strength estimation of Roller-Compacted concrete with recycled aggregates, Mathematics 12 (16) (2024) 2542.
[85] L. Shang, H.F. Isleem, W.J. Almoghayer, M. Khishe, Prediction of ultimate strength and strain in FRP wrapped oval shaped concrete columns using machine learning, Sci. Rep. 15 (1) (2025) 10724.
[86] A. Kapil, K. Jadda, A.A. Jee, Developing machine learning models to predict the Fly ash concrete compressive strength, Asian J. Civ. Eng. 25 (7) (2024) 5505–5523.
[87] S. Sathvik, et al., Modelling the mechanical properties of concrete produced with polycarbonate waste ash by machine learning, Sci. Rep. 14 (1) (2024) 11552.
[88] D.R. Kumar, P. Kumar, P. Thangavel, W. Wipulanusat, C. Thongchom, P. Samui, Optimized machine learning models for predicting the tensile strength of high-performance concrete, J. Struct. Integr. Maint. 10 (1) (2025) 2471682.
[89] Q.-H. Le, D.-H. Nguyen, T. Sang-To, S. Khatir, H. Le-Minh, A.H. Gandomi, T. Cuong-Le, Machine learning based models for predicting compressive strength of geopolymer concrete, Front. Struct. Civ. Eng. 18 (7) (2024) 1028–1049.
[90] V. Vakharia, R. Gujar, Prediction of compressive strength and portland cement composition using cross-validation and feature ranking techniques, Constr. Build. Mater. 225 (2019) 292–301.
[91] H. Erdal, M. Erdal, O. Simsek, H.I. Erdal, Prediction of concrete compressive strength using non-destructive test results, Comput. Concr. 21 (4) (2018) 407–417.
[92] S. Nazar, J. Yang, W. Ahmad, M.F. Javed, H. Alabduljabbar, A.F. Deifalla, Development of the new prediction models for the compressive strength of nanomodified concrete using novel machine learning techniques, Buildings 12 (12) (2022) 2160.
[93] M. Nafiuzzaman, T.I. Jakir, I.J. Aditi, A. Kabir, K.A. Ahsan, Different machine learning approaches to predict the compressive strength of composite cement concrete, J. Build. Pathol. Rehabil. 10 (2) (2025) 1–22.
[94] M.M. Alsaadawi, M.K. Elshaarawy, A.K. Hamed, Concrete compressive strength classification using hybrid machine learning models and interactive GUI, Innov. Infrastruct. Solut. 10 (5) (2025) 1–29.
[95] M. Ozdemir, G. Celik, Classification of concrete compressive strength using machine learning methods. in International Conference on Cooperative Design, Visualization and Engineering, Springer, 2024, pp. 343–353.
[96] B. Pooraskarparast, S.N. Dang, V. Pakrashi, J.C. Matos, Performance of Fine-Tuning techniques for multilabel classification of surface defects in reinforced concrete bridges, Appl. Sci. 15 (9) (2025) 4725.
[97] S. Kim, K. Oh, J. Shin, Machine Learning-Based rapid prediction method of failure mode for reinforced concrete column, J. Earthq. Eng. Soc. Korea 28 (2) (2024) 113–119.
[98] X. Chen, X. Zhang, W.-Z. Chen, Advanced predictive modeling of concrete compressive strength and slump characteristics: a comparative evaluation of BPNN, SVM, and RF models optimized via PSO, Materials 17 (19) (2024) 4791.
[99] X. Liu, S. Wang, B. Liu, Q. Liu, Y. Zhou, J. Chen, J. Luo, Cement-based grouting material development and prediction of material properties using PSO-RBF machine learning, Constr. Build. Mater. 417 (2024) 135328.
[100] F. Ergen, M. Katlav, Investigation of optimized machine learning models with PSO for forecasting the shear capacity of steel fiber-reinforced SCC beams with/out stirrups, J. Build. Eng. 83 (2024) 108455.
[101] Y. Zhang, Y. Jiang, C. Li, C. Bai, F. Zhang, J. Li, M. Guo, Prediction of cement-stabilized recycled concrete aggregate properties by CNN-LSTM incorporating attention mechanism, Mater. Today Commun. 42 (2025) 111137.
[102] X. Bai, R. Zhang, J. Le, B. Li, W. Fu, S. Jia, W. Yin, An intelligent algorithm based on the improved CNN-LSTM for the detection of concrete reinforcement information, Prog. Electromagn. Res. M 130 (2024).
[103] P. Das, A. Kashem, M. Islam, A. Ahmed, M.A. Haque, M. Khan, Alkali-activated binder concrete strength prediction using hybrid-deep learning along with shapely additive explanations and uncertainty analysis, Constr. Build. Mater. 435 (2024) 136711.
[104] H.D. Nguyen, C. Kim, Y.-J. Lee, M. Shin, Incorporation of machine learning into multiple stripe seismic fragility analysis of reinforced concrete wall structures, J. Build. Eng. 97 (2024) 110772.
[105] M. Hosseinzadeh, H. Samadvand, A. Hosseinzadeh, S.S. Mousavi, M. Dehestani, Concrete strength and durability prediction through deep learning and artificial neural networks, Front. Struct. Civ. Eng. 18 (10) (2024) 1540–1555.
[106] A. Alishvandi, J. Karimi, S. Damari, A. Moayedi Far, M. Setodeh Pour, M. Ahmadi, Estimating the compressive strength of plastic concrete samples using machine learning algorithms, Asian J. Civ. Eng. 25 (2) (2024) 1503–1516.
[107] Y. Peng, C. Unluer, Interpretable machine learning-based analysis of hydration and carbonation of carbonated reactive magnesia cement mixes, J. Clean. Prod. 434 (2024) 140054.
[108] N. Ngoc-Mai and M.T. Cao, Predicting Mechanical Properties of Concrete Structures Using Metaheuristic Optimization-Based Machine Learning Models, Available at SSRN 4923416.
[109] Y. Tang, C. Zhou, W. Wang, W. Zhang, Y. Cheng, Machine learning driven bond performance prediction between FRP bars and coral aggregate concrete, Constr. Build. Mater. 442 (2024) 137684.
[110] B. Li, et al., Prediction model of maximum stress for concrete pipes based on XGBoost-PSO algorithm, in: Structures, 68, Elsevier, 2024.
[111] F.M. Wani, J. Vemuri, R. Chenna, Prediction of storey drift for reinforced concrete structures subjected to pulse-like ground motions using machine learning classification models, Int. J. Struct. Integr. 15 (3) (2024) 409–433.
[112] M.S. Thakur, S.M. Pandhiani, V. Kashyap, A. Upadhya, P. Sihag, Predicting bond strength of FRP bars in concrete using soft computing techniques, Arab. J. Sci. Eng. 46 (2021) 4951–4969.
[113] K. Khan, M. Iqbal, F.E. Jalal, M.N. Amin, M.W. Alam, A. Bardhan, Hybrid ANN models for durability of GFRP rebars in alkaline concrete environment using three swarm-based optimization algorithms, Constr. Build. Mater. 352 (2022) 128862.
[114] C. Jin, Y. Qian, S.A. Khan, W. Ahmad, F. Althoey, B.S. Alotaibi, M.A. Abuhussain, Investigating the feasibility of genetic algorithms in predicting the properties of eco-friendly alkali-based concrete, Constr. Build. Mater. 409 (2023) 134101.
[115] S. Khursheed, J. Jagan, P. Samui, S. Kumar, Compressive strength prediction of Fly ash concrete by using machine learning techniques, Innov. Infrastruct. Solut. 6 (3) (2021) 149.
[116] M. Owais, L.K. Idriss, Modeling Green recycled aggregate concrete using machine learning and variance-based sensitivity analysis, Constr. Build. Mater. 440 (2024) 137393.
[117] K. Li, Y. Long, H. Wang, Y.-F. Wang, Modeling and sensitivity analysis of concrete creep with machine learning methods, J. Mater. Civ. Eng. 33 (8) (2021) 04021206.
[118] A. Yazdani, A. Nicknam, E.Y. Dadras, S.N. Eftekhari, Entropy-based sensitivity analysis of global seismic demand of concrete structures, Eng. Struct. 146 (2017) 118–126.
[119] L.K. Idriss, M. Owais, Global sensitivity analysis for seismic performance of shear wall with high-strength steel bars and recycled aggregate concrete, Constr. Build. Mater. 411 (2024) 134498.
[120] I.K. Harith, W. Nadir, M.S. Salah, M.L. Hussien, Prediction of high-performance concrete strength using machine learning with hierarchical regression, Multiscale Multidiscip. Model. Exp. Des. 7 (5) (2024) 4911–4922.
[121] K. Kaptan, S. Cunha, J. Aguiar, A review: construction and demolition waste as a novel source for CO2 reduction in portland cement production for concrete, Sustainability 16 (2) (2024) 585.
[122] Y. Lu, J. Xiao, Y. Li, 3D printing recycled concrete incorporating plant fibres: a comprehensive review, Constr. Build. Mater. 425 (2024) 135951.

[123] B. Zhou, M. Zhang, G. Ma, An experimental study on 3D printed concrete reinforced with fibers recycled from wind turbine blades, J. Build. Eng. 91 (2024) 109578.
[124] P.S. Humbert, J. Castro-Gomes, CO2 activated steel slag-based materials: a review, J. Clean. Prod. 208 (2019) 448–457.
[125] J. Zhou, H. Shang, L. Fan, X. Wang, Y. Huang, Experimental investigation on Nano-Al2O3 and hydroxypropyl methyl cellulose (HPMC) modified cement-based coatings for corrosion resistance, J. Build. Eng. 95 (2024) 110216.
[126] M.K. Elshaarawy, M.M. Alsaadawi, A.K. Hamed, Machine learning and interactive GUI for concrete compressive strength prediction, Sci. Rep. 14 (1) (2024) 16694.
[127] U. Pulkit, S.D. Adhikary, Development of a novel GUI-Based computer program for predicting the temperature distribution in the concrete compartment and member, J. Struct. Des. Constr. Pract. 30 (1) (2025) 04024086.
[128] M. Katlav, F. Ergen, I. Donmez, AI-driven design for the compressive strength of ultra-high performance geopolymer concrete (UHPGC): from explainable ensemble models to the graphical user interface, Mater. Today Commun. 40 (2024) 109915.
[129] H. Alabduljabbar, F. Farooq, M. Alyami, A.W. Hammad, Assessment of the split tensile strength of fiber reinforced recycled aggregate concrete using interpretable approaches with graphical user interface, Mater. Today Commun. 38 (2024) 108009.
[130] M. Alyami, M. Khan, M. Fawad, R. Nawaz, A.W. Hammad, T. Najeh, Y. Gamil, Predictive modeling for compressive strength of 3D printed fiber-reinforced concrete using machine learning algorithms, Case Stud. Constr. Mater. 20 (2024) e02728.
[131] M. Hambach, M. Rutzen, D. Volkmer, Properties of 3D-printed fiber-reinforced portland cement paste. in 3D concrete printing technology, Elsevier, 2019, pp. 73–113.
[132] M. Alyami, M. Khan, M.F. Javed, M. Ali, H. Alabduljabbar, T. Najeh, Y. Gamil, Application of metaheuristic optimization algorithms in predicting the compressive strength of 3D-printed fiber-reinforced concrete, Dev. Built Environ. 17 (2024) 100307.
[133] M.N. Uddin, F. Mahamoudou, B.-Y. Deng, M.M.E. Musa, L.W.T. Sob, Prediction of rheological parameters of 3D printed polypropylene fiber-reinforced concrete (3DP-PPRC) by machine learning, Mater. Today. Proc. (2023).
[134] N.T. Nguyen, T.-T. Bui, Q.-B. Bui, Fiber reinforced concrete for slabs without steel rebar reinforcement: assessing the feasibility for 3D-printed individual houses, Case Stud. Constr. Mater. 16 (2022) e00950.
[135] K. Kopitha, P. Rajeev, J. Sanjayan, Y. Elakneswaran, CO2 sequestration and low carbon strategies in 3D printed concrete, J. Build. Eng. (2024) 111653.
[136] S.D. Datta, M.K. Akon, M.R.I. Nayan, and S. Ahmed, Sustainable production of 3D printed concrete in the construction industry based on compressive strength and embodied CO2 analysis, 2024.
[137] B. Bodur, et al., Durability of Green rubberized 3D printed lightweight cement composites reinforced with micro attapulgite and micro steel fibers: printability and environmental perspective, J. Build. Eng. 90 (2024) 109447.
[138] Y. Zhang, Q. Zhang, A.H. AlAteah, A. Essam, S.A. Mostafa, Predictive modeling for mechanical characteristics of ultra high-performance concrete blended with eggshell powder and nano silica utilizing traditional technique and machine learning algorithm, Case Stud. Constr. Mater. 21 (2024) e04025.
[139] H. Izadgoshasb, A. Kandiri, P. Shakor, V. Laghi, G. Gasparini, Predicting compressive strength of 3D printed mortar in structural members using machine learning, Appl. Sci. 11 (22) (2021) 10826.
[140] Y. Weng, M. Li, D. Zhang, M.J. Tan, S. Qian, Investigation of interlayer adhesion of 3D printable cementitious material from the aspect of printing process, Cem. Concr. Res. 143 (2021) 106386.
[141] Y. Chen, S. He, Y. Zhang, Z. Wan, O. Çopuroğlu, E. Schlangen, 3D printing of calcined clay-limestone-based cementitious materials, Cem. Concr. Res. 149 (2021) 106553.